Robot-assisted ultrasound navigation platform for 3D HIFU treatment planning: Initial evaluation for conformal interstitial ablation

L. Daunizeau, A. Nguyen, M. Le Garrec, J.Y. Chapelon, W.A. N'Djin

Robot-assisted Ultrasound Navigation Platform for 3D HIFU treatment planning: initial evaluation for conformal interstitial ablation

L. Daunizeau*[1], A. Nguyen[1], M. Le Garrec[1], J.Y. Chapelon[1], W.A. N'Djin[1]

[1] LabTAU, INSERM, Centre Léon Bérard, Université Lyon 1, Univ Lyon, F-69003, Lyon, France

*e-mail: loic.daunizeau@inserm.fr

Abstract

Interstitial Ultrasound-guided High Intensity Focused Ultrasound (USgHIFU) therapy has the potential to deliver ablative treatments which conform to the target tumor. In this study, a robot-assisted US-navigation platform has been developed for 3D US guidance and planning of conformal HIFU ablations. The platform was used to evaluate a conformal therapeutic strategy associated with an interstitial dual-mode USgHIFU catheter prototype (64 elements linear-array, measured central frequency f = 6.5 MHz), developed for the treatment of HepatoCellular Carcinoma (HCC). The platform included a 3D navigation environment communicating in real-time with an open research dual-mode US scanner/HIFU generator and a robotic arm, on which the USgHIFU catheter was mounted. 3D US-navigation was evaluated *in vitro* for guiding and planning conformal HIFU ablations using a tumor-mimic model in porcine liver. Tumor-mimic volumes were then used as targets for evaluating conformal HIFU treatment planning in simulation. Height tumor-mimics (ovoid- or disc-shaped, sizes: 3 – 29 cm^3) were created and visualized in liver using interstitial 2D US imaging. Robot-assisted spatial manipulation of these images and real-time 3D navigation allowed reconstructions of 3D B-mode US images for accurate tumor-mimic volume estimation (relative error: 4 ± 5 %). Sectorial and full-revolution HIFU scanning (angular sectors: 88–360°) could both result in conformal ablations of the tumor volumes, as soon as their radii remained ≤ 24 mm. The presented US navigation-guided HIFU procedure demonstrated advantages for developing conformal interstitial therapies in standard operative rooms. Moreover, the modularity of the developed platform makes it potentially useful for developing other HIFU approaches.

Keywords: Dual-mode interstitial ultrasound, ultrasound imaging, HIFU therapy, conformal ablation, treatment planning, 3D navigation guidance, robot-assisted procedure

1 Introduction

Minimally invasive therapies represent an alternative to open surgery with potential benefits given that only small incisions are performed, which limits the risk of infection, reduces patient recovery time and pain. Oncology has benefited from those techniques and minimally invasive ablative procedures have been developed to treat local tumor. Thermal ablation procedures rely on interstitial probes which are inserted inside or adjacent to the tumor, and locally modify the temperature of surrounding tissues up to a lethal threshold. Typical probes used in a clinical context either increase temperature: Radio Frequency Ablation (RFA)[1], [2], Microwave Ablation (MWA)[3]–[5], Laser Induced Thermal Therapy (LITT)[6], [7] or decrease temperature (Cryoablation)[8]. However, these technics rely on physical principles that limit their ability to modify temperature on a precise area. During cryoablation procedure, temperature modifications around the probe are driven by thermal diffusion[9], which is dependent on tissue thermal properties and cannot be controlled. For RFA and MWA procedures, thermal diffusion is preponderant in the extension of the thermal ablation, although the temperature increases also depend on the energy deposited in tissues by absorption of the electromagnetic energy radiated by the probe[10]–[12]. During LITT procedures, a beam of photons is carried by an optical fiber and spread by a diffusor directly inside the tumor[13]. Photons are rapidly absorbed by tissues and the spatial extension of the thermal heating is mostly driven by thermal diffusion, resulting in thermal ablations having cylindrical to ellipsoidal shapes around the probe[14]. Consequently, these mentioned interstitial treatment modalities do not allow conformal ablation of target volumes with complex asymmetric shapes, as can be often observed with solid tumors. Furthermore, large volume of healthy tissues may be ablated outside the diseased tissues, with potential side effects for the patient. Finally, if critical tissues must be spared, such as nerves, blood vessel or brain areas for transcranial procedures, the lack of treatment conformation may also limit the use of previously cited minimally invasive thermal ablation procedures, and reduce the number of patients eligible for such therapies.

The ability of ultrasound (US) waves to generate thermal ablations in tissues has been investigated since the early 40s[15] and developed in the 50s especially with the work of Fry[16], [17]. In human soft tissues, ultrasound waves emitted at several MHz (wavelength: 100s of micrometers) can be focused very precisely in the body (millimeter-scale focal region) and energy deposition in tissues may be limited to the focal region, where pressure amplitudes are the highest[18]. Furthermore, by focusing US energy, temperatures above 55°C

are reached within seconds at the focal point, minimizing the perfusion dependency of the treatment. Ultrasound focusing can be created either by the transducer shape (natural focusing), by adding acoustic lenses at the front of the transducer to refocus the wavefront, or by driving a multi-element phased-array transducer with appropriate time delayed electrical signals (electronic focusing). Ultrasound focusing ability has the potential to overcome some of the challenges faced with current interstitial thermal ablation technics for achieving conformal treatments. The location of the US energy deposition can be controlled and the shape of the ablated area can be adapted in accordance with patient specific anatomy. Over the last decades, several High Intensity Focused Ultrasound (HIFU) devices have been developed and used in a clinical context to ablate localized tissues (e.g. tumors) in different organs[19]–[28]. Given their size, HIFU devices are generally extracorporeal or endocavitary. These devices have the advantage of being non- or minimally- invasive. However, it remains complex to use an extracorporeal device to treat tumor far from skin surface as heterogeneous media modify ultrasound wave path and reduce significantly the pressure amplitude at the focal point. For instance, phase aberrations may be induced by fat layers (speed of sound: ~1450 $m.s^{-1}$), which may need to be taken into account and corrected at the focal point[29]. Also acoustic barrier such as bones (rib cage, skull) or gas (lung, bowel) may limit the reachable ablation area of extracorporeal HIFU devices[30]. Considering these many challenges, intraoperative HIFU therapies have also showed particular interest during open procedures, as a complementary tool to surgery [31].

In this context, endovascular or interstitial approaches can exhibit several advantages, by offering minimally-invasive alternatives where catheter based ultrasound devices are placed close to or directly in contact with the target tumor to be ablated[32], [33]. Given the mandatory compact design of interstitial devices, catheter based ultrasound transducers are generally made of a few independent elements, reducing the focusing capability of those devices[34]–[37]. Recent technological improvements have allowed the creation of miniaturized dual-mode transducer with a higher number of independent elements capable of both therapy and imaging[38]–[40]. Those transducers are linear arrays allowing electronic focusing for both imaging and therapy modes. Hence, dual-mode catheter based ultrasound probe have the potential to create a conformal thermal ablation of solid tumor that would not be easily reachable by extracorporeal HIFU devices. In this work, we used an interstitial dual-mode ultrasound prototype intended for studying new strategies for

treating hepatocellular carcinoma (HCC), the main primary cancer of the liver, an organ surrounded by the rib cage and hence not easily accessible by extracorporeal HIFU devices.

As with extracorporeal HIFU devices, focal points generated by interstitial HIFU devices must be juxtaposed with each other to treat an entire tumor volume. Thus, to generate a conformal treatment, it is mandatory to know precisely the shape of the tumor in order to plan the position of the focal points accordingly. During treatment, the evolution of thermal lesion must also be monitored to ensure that the target volume is correctly ablated and that there is no damage to healthy tissues. The same imaging modality is generally used for both treatment planning imaging and treatment monitoring. The two imaging modalities mainly used for HIFU guidance are Magnetic Resonance (MR) Imaging and US imaging[41], [42]. MR imaging has the advantage of providing 3D volumes of the anatomical structures which can be used directly for the treatment planning phase[43]. During HIFU treatment execution, MR imaging can also provide real time tissue temperature feedback which allows precise control of the treatment evolution in 3D[44], [45]. However, in order to work in this specific strong magnetic environment and not generate artifacts on the MR images, MR-compatible HIFU devices must be designed with additional constraints on the magnetic properties (magnetic susceptibility) of the components used. Also, MR imaging is expensive and not easily accessible, which limits the use of MR-guided HIFU (MRgHIFU) protocols. Ultrasound-guided HIFU (USgHIFU) represent an alternative to MRgHIFU. Yet conventional US imaging probes can only reconstruct 2D images. In order to allow 3D conformal treatment planning, the US imaging probe must be displaced so that the 2D images may scan the whole targeted volume[25]. US imaging can also be used to monitor the treatment in real-time, as tissue echogenicity changes may appear where the energy is concentrated[28], [46]. Other ultrasound based method for treatment monitoring have been investigated such as ultrasound thermometry, change in backscatter energy or elastography[47]–[49]. To date, even though these methods are not as established as MRI thermometry, they show promise in providing real-time assessment of thermal ablation treatment, with spatial resolution on a submillimetric scale, in a standard non-magnetic operative room, and at a lower cost.

In the context of interstitial USgHIFU conformal therapies, the development of dual-mode ultrasound catheters, i.e. capable of therapy and imaging, may help address some of the challenges identified above and especially the capacity of an interstitial device to deliver a conformal treatment. Such probes can focus the ultrasound in 2D while providing in-situ US images usable for both 2D treatment planning and monitoring[50],

[51]. To date, however, the performance of conformal USgHIFU ablation involving complex 3D treatment planning is not available in clinic, since it would require imaging and treating the target tissues in 3D. In this work, we present the initial evaluation of a robot-assisted US navigation platform for allowing the 3D treatment planning of interstitial USgHIFU conformal therapies of HCC. The interest of combining dual-mode interstitial ultrasound technologies with robotics and virtual navigation for medicine has been studied, in order to demonstrate the technical feasibility of precisely guiding conformal HIFU therapies using 3D US navigation imaging.

2 Materials and Methods

2.1 Ultrasound Navigation for interstitial HIFU planning: principle

In conventional interstitial procedures (Radiofrequency, Microwave, Cryotherapy) for thermal ablation of localized tumors, a probe (e.g. needle, catheter) is inserted inside the tumor under image guidance. For the treatment of HCC, the interstitial device insertion is guided in real-time using extracorporeal US imaging. Once the probe is in position, the ablation starts and extends omni-directionally at a rate depending on the nature of the tissue and probe performances. The treatment lasts until the thermal ablation has covered the entire tumor volume with additional security margins. These techniques do not allow directing the ablation toward specific preselected tissue regions. HIFU alternative procedures use directional energy absorption phenomenon in order to extend the ablation volume (along the ultrasound propagation direction), while allowing spatial tissue selection. These procedures require defining a HIFU treatment planning, in order to determine precisely a set of HIFU focal points (position, ultrasound energy disposition) prior to the actual treatment. Once inserted in the tumor, the HIFU catheter is driven to focus the ultrasound beam on each focal point predefined in the 3D treatment planning.

In order to achieve a conformal HIFU treatment, these focal points must be predefined to generate an ablation fitting to the target volumetric shape. It is thus mandatory to know precisely the 3D shape of the tumor, its relative position with respect to the probe and to be able to manipulate these data in real-time for guiding the HIFU treatment execution. In the presented study, 3 specific steps have been identified to deliver a conformal interstitial HIFU treatment: i) to determine the 3D shape of the target volume to be ablated using 3D US imaging reconstructions. The probe was displaced by the robot while 2D US images were generated by an US scanner. Both information were stored and reused by the volume reconstruction algorithm ii) to compute

automatically a conformal HIFU treatment planning based on the previously determined target volume. Manual segmentation of the targeted volume was performed using the 3D navigation interface and used as the target volume by the treatment planning software iii) to execute and monitor the corresponding conformal HIFU treatment as defined at step ii). The probe was displaced by the robot and HIFU sequences were generated using a power amplifier driving system (**Fig. 1**). To execute each of these 3 steps and study the interest of US-image based Navigation guidance for HIFU therapy, a robot-assisted, dual-mode ultrasound platform (the US scanner and power amplifier functions are merged in a single system) has been developed. In the presented work, the first 2 steps have been evaluated experimentally, while the last step has been investigated in simulation in order to validate the concept.

2.2 Robot-assisted US-navigation guided HIFU platform

The platform was made of 5 components (**Fig. 2**). The 1st component was an open research ultrasound scanner (Vantage 256, Verasonics, United States) with 256 independent emission/reception channels. The scanner was a dual-mode US scanner/HIFU driving system platform which allowed piloting dual-mode ultrasound devices both in US imaging modes (e.g. standard B-mode) using transient wave (TW) regimes, and HIFU therapy modes using continuous wave (CW) regimes. In this work, an USgHIFU interstitial approach was studied using a prototype (2nd component) developed for conformal ablations of liver tumors. The 3rd component of the platform was an US-image based navigation station developed using open source programs providing tools and algorithms for visualization, reconstruction and treatment execution[52], [53]. The station was embedded on a laptop computer and included a data communication and reconstruction tool, PlusToolKit (https://plustoolkit.github.io/), natively compatible with the 3D virtual environment tool 3DSlicer (http://www.slicer.org), and a HIFU treatment planning tool. This station allowed 3D US image reconstruction from 2D US image series, real-time fusion between US images, the interstitial prototype CAD (Computer Aided Design) model, target volume segmentations (e.g. tumor) and automatic HIFU treatment planning. The 4th component of the platform was a 7 axis robot (LBR IIWA, KUKA, Germany) on which the USgHIFU prototype was mounted. The robot assured a dual role by providing the prototype position in real-time, while displacing it to the commanded positions. Finally, the last component was a HIFU modeling environment (CIVA medical, recent evolution of in-house created modeling software ABLASIM[54], CEA/LabTAU, France) embedded on a

separated desktop computer. GPU were used for parallel calculations and fast simulations of realistic HIFU sequence strategies (planning) provided by the navigation platform.

2.3 Real-time US navigation: data communication

The US scanner, robotic arm and navigation station were all connected on the Local Area Network (LAN) and used TCP/IP protocol for communication and data exchange. Data transferred complied with the OpenIGTLink (http://openigtlink.org/) data structure[55]. 2D US images were provided by the dual-mode prototype and transferred in real-time from the US scanner to the navigation station. In order to provide the US scanner with data exportation functionality, a 1st implementation of the OpenIGTLink protocol was developed (in Matlab). Series of 2D US images (data stream #1) were sent in real-time on the local network using TCP/IP protocol. In parallel, the positions of the 2D US images in the 3D space were updated in real-time on the navigation station, by converting the robot position (matrix of transformation) and considering solid connection between the robot, the prototype and the US image. A 2nd implementation of the OpenIGTLink protocol was written (in Java) to program the robot with a background task running a TCP/IP server. This server sent the robot flange position in real-time (data stream #2) to the navigation station. The PlusToolKit reconstruction algorithm embedded in the navigation station allowed receiving these 2 data streams in real-time: the series of 2D B-mode US images (data stream #1) and their positions in the 3D space (data stream #2, transformed from robotic arm position) (**Fig. 2**). A configuration file (xml format) was written so the US-navigation station (PlusToolKit) could know the TCP/IP addresses of the US scanner and the robot, and differentiate the type of data exported by each component of the platform. Based on the 2 data streams received in real-time, a 3D volume reconstruction was performed (PlusToolKit algorithm) and the resulting data was transferred to the 3D virtual environment tool (3DSlicer). The reconstructed 3D US-image was then displayed in the virtual environment for further analyzes.

2.4 Dual-mode interstitial USgHIFU prototype

The dual-mode USgHIFU prototype (Vermon, France) was made of a 3-mm diameter stainless steel catheter with a 64-elements linear array ultrasound transducer, 13.1 mm x 2.0 mm (element pitch: 205 µm), mounted at its tip (**Fig. 3a**). The catheter was 20 cm long. The theoretical specifications for the dual-mode ultrasound transducer were a central frequency of 6.0 MHz (±10%) and a maximum acoustic intensity (I_{ac}) ≤ 20 $W.cm^{-2}$. The central frequency measured on the prototype involved in the experimental study was 6.5 MHz. In

therapy mode (CW), the reachable acoustic intensity was of 20 W/cm^2 (manufacturer data). A compromise between imaging and therapy performances was made by not covering the dual-mode transducer with any acoustic lens in order to maximize the output acoustic power transfer and reduce self-heating of the device in HIFU mode. The prototype could dynamically focus ultrasound over distances ranging 6-20 mm (ultrasound propagation direction, r-axis) and over steering distances ranging ± 6 mm (z-axis). In imaging mode (TW), the impulse response duration was given at 250 ns at -6 dB and 700 ns at -20 dB (manufacturer data). The frequency bandwidth at -6 dB (from the Fourier transform of the impulse response) was of 60% (frequency range: 4.6 – 8.5 MHz). In order to keep optimal imaging and therapeutic capabilities of dual-mode USgHIFU prototypes, some studies had previously proposed to switch electronically between 2 driving circuits, dedicated either to imaging or therapy (matching circuit) modes[50], [51]. In the current study, given the low level of active electrical power needed on each channel (~0.2 W) to produce high intensity ultrasound with one element, no electrical impedance matching circuit has been added to the prototype.

2.5 In-vitro liver tumor-mimic model

A tumor-mimic model was used to study the performances of the US-navigation guided HIFU platform. This model implanted in liver tissues was previously shown to be visible on US images (both in-vitro an in-vivo) as a well delimited hyperechoic region, while exhibiting an ultrasound attenuation similar to those of tissues around 3-MHz HIFU therapeutic frequencies[56], [57]. Tumor-mimics were composed of agarose (Agarose for routine use®, Sigma-Aldrich, Steinheim, Germany), cellulose (Fibrous, medium cellulose®, Sigma-Aldrich Steinheim, Germany), glycerol (Anhydrous glycerol®, Fluka, Buchs, Switzerland), methylene blue (Methylene blue hydrate®, Sigma-Aldrich, Steinheim, Germany) and sterile water. The mixture, prepared as described in the study of Scott et al. (2000)[58] was liquid at 65°C and solid at 37°C. Therefore, the tumor-mimic can be injected in warm liquid phase directly in liver tissues at 65°C and then polymerized when cooling down to liver tissue temperature (≤ 37°C). The injectable approach, however, limited the tumor-mimic diameter to ~1 cm due to the liver compressibility, which was sufficient for studying liver metastases HIFU treatments[57]. In the current study, an alternative solution was proposed to reach higher tumor-mimic diameters and evaluate the USgHIFU platform in the context of hepatocellular carcinoma (HCC) interstitial ablations. It consisted in creating soft molds (modeling clay) of various shapes, and in injecting the warm solution through the molds. After cooling down and polymerization, tumor-mimics of several centimeters in diameter were released from their

molds. For each experimental trial, a tissue piece was extracted from an in-vitro heifer liver sample and replaced by inserting the solid tumor-mimic model. Eight tumor-mimics were made. The USgHIFU prototype was inserted either inside or adjacent to the tumor-mimic volume (**Fig. 3**). Then, the 3 steps of the treatment procedure were evaluated: i) the determination of the tumor-mimic 3D shape, ii) the definition of a conformal HIFU treatment planning and iii) the execution in simulation of the corresponding HIFU treatment.

2.6 3D geometry of the target tumor

The 1st step of the procedure was the determination of the target geometry. The navigation platform was used to reconstruct a 3D US volume containing the HCC tumor-mimic models and surrounding in-vitro liver tissues. Real-time 2D B-mode US imaging was performed with the interstitial prototype working in imaging mode, delivering pulses (TW) with a central frequency of 6.3 MHz (**Fig. 3c**). This was the closest frequency to the measured central frequency of the transducer (6.5 MHz), which could be generated by the ultrasound scanner. Sectorial 2D images (angular aperture α = ± 30°, imaging depths: 40-50 mm, depending on the tumor-mimic distance to the probe axis) were reconstructed using plane-waves compounding sequences (11 multi-angle plane waves, angular increment $d\alpha$ = 6.8°, frame rate: 10 images/s). B-mode US volumes were reconstructed from series of 2D B-mode US images acquired in-situ in multiple positions in order to scan surrounding tissues in the 3D space (Plus Toolkit reconstruction algorithm). The procedure was performed by moving the interstitial prototype with the robotic arm while recording its position in space. A robot application was written to command precisely rotations and translations of the prototype, respectively around and along the elevational z-axis. The scanning process was divided in separate stages. The prototype was translated to the most distal part of the tumor-mimic and a rotation of $\theta \leq 360°$ was performed. After a 1st rotational scan, if the whole extent of the tumor-mimic was not imaged in the elevational dimension, the prototype was translated of a step $\Delta z = 18$mm in its proximal direction and a 2nd rotational scan was performed. The process was repeated until the whole tumor-mimic volume was scanned and enclosed in the reconstructed 3D US image volume. Then, manual segmentations of the tumor-mimic 3D shapes were performed plan by plan, using the segmentation tools provided by the navigation station. Tumor-mimic segmentations could be uploaded in post-processing from the navigation station to the HIFU simulation environment.

2.7 Conformal HIFU treatment planning

The 2nd step of the procedure was the conformal treatment planning. The HIFU parameters were automatically determined according to the 3D shape of the HCC tumor-mimic model (provided by the previous segmentation step), the location of the USgHIFU prototype insertion (positioning matrix) and HIFU simulations. A dedicated algorithm (written in Matlab) embedded on the US-navigation platform had 2 main parts. The 1st part allowed determining automatically the number (n), and positions (r, θ, z) of the HIFU focal points to entirely scan the surface of the tumor. The 2nd part assigned a HIFU exposure duration (t_{ON} / t_{OFF}) for each focal point based on preliminary tuning (HIFU simulations), in order to achieve a conformal thermal ablation of the target tumor.

2.7.1 HIFU exposure time tuning

Preliminary tuning in simulation allowed anticipating elementary HIFU ablation performances when driving the USgHIFU prototype in CW mode. These tuning considered the standard strategies adopted to avoid transducer damage due to self-heating in CW mode: i) the presence of a water-cooling system around the transducer (water temperature: 20°C); ii) the driving of the transducer at its resonance frequency (close to the central frequency for the presented prototype) to ensure the best electro-acoustic efficiency. The driving frequency of the USgHIFU prototype was kept constant in simulation, regardless of the focusing depth, to further preserve the transducer integrity during future HIFU experiments. Preliminary simulations of the theoretical HIFU performances were conducted using the mean theoretical specifications of the USgHIFU catheter design: f = 6.0 MHz, I_{ac} = 20 W.cm^{-2}. In these conditions, pre-tuning simulations showed that heat deposition rates in liver tissues were acceptable up to a focusing depth of 20 mm. Elementary ablations were simulated by applying single and continuous HIFU exposures at a given focal distance. All combinations of dynamic ultrasound focusing over distances ranging 6-20 mm (ultrasound propagation direction, r-axis) and steering distance of ± 6 mm (z-axis) were simulated. The maximum acoustic intensity achievable at the surface of the transducer was 20 W.cm^{-2} in CW mode (manufacturer specifications). To minimize the duration of the overall treatment procedure, all HIFU performances were simulated in the most favorable conditions of maximum acoustic intensity (20 W.cm^{-2}). The exposure time of each single exposure was set during pre-tuning simulations, such that the maximum temperature in tissues did not reach 100°C. Above this temperature limit, additional boiling effects modify the ultrasound propagation in a way which is not accounted by the model

used. The resulting elementary ablation, tissue area exhibiting an equivalent time at 43°C (or thermal dose) t_{43} ≥ 240 CEM (Cumulative Equivalent Minutes), was a homogenous triangle started from the transducer and ending at the focal point (**Fig. 4**). Therefore, planning homogenous 3D conformal ablations with this prototype was done by determining a distribution of HIFU focal points located only on the 3D surface of the target volume (e.g. tumor-mimic). An abacus was created, t_{43} (r, z, t), to determine the minimum exposure duration t_{ON} required to achieve similar homogenous elementary ablations for all configuration of HIFU targeting involved in the 3D conformal treatment planning of a tumor-mimic.

2.7.2 HIFU focusing positions and trajectories

The focal point positioning strategy was driven by the idea that each HIFU exposure should benefit equally from the thermal diffusion arising from the previous exposure. The objective was to anticipate thermal diffusion effects in order to smooth the ablated volume shape and avoid overheated areas. Focal points positions were then calculated to follow a zig-zag trajectory on the 3D surface of the tumor-mimic. The shape of this trajectory was driven by the tumor geometry and the HIFU focusing capability of the interstitial prototype. The tumor volume was first divided in several stages along its elevation (prototype insertion z-axis). Given the HIFU beam steering capabilities of the prototype (± 6 mm in elevation, z-axis), 1 tumor stage was sized with a 10-mm elevation. Each tumor stage was split in tumor angular sectors (angular step: 15°). To treat a given angular sector, a 3D zig-zag HIFU trajectory was defined to scan the 3D boundary facing the prototype. This 3D zig-zag trajectory was achieved with 2D dynamic focusing (r- and z- axis) and prototype back-and-forth mechanical rotations. The algorithm calculated the HIFU focal distances by considering the distances between the interstitial prototype and the most distant part of the tumor along the rOz plan. This approach allowed managing both cases of prototype insertions: inside and beside the tumor. The HIFU exposure durations were determined according to the pre-calculated abacus. The abacus covered distances from 6 to 20 mm. Therefore, focal points < 6 mm and > 20 mm were assigned exposure durations identical to the 6-mm and 20-mm cases respectively. This procedure was repeated for each angular sector of a given tumor stage, and for each stage, starting from the lowest (distal part, along the insertion z-axis). One tumor stage was then treated by avoiding mechanical translations of the prototype along its insertion axis, which could cause tumor cells dissemination. The next tumor stage treatment started once the previous one was entirely treated. Finally, a full treatment planning could be achieved by limiting the number of mechanical translations of the prototype.

2.8 HIFU treatment execution

The final step of the procedure was the execution of the corresponding conformal HIFU treatment. The presented platform and developed architecture allowed executing a conformal HIFU treatment planning both in simulation and experimentally. In this paper, conformal HIFU tumor ablation was evaluated in simulation only. The algorithm managing the conformal HIFU treatment planning made a correspondence between the set of HIFU focal points and their associated exposure durations (t_{ON} / t_{OFF}) based on their positions (r, θ, z) and the thermal dose abacus, t_{43} (r, z, t), determined earlier. The full treatment planning was then re-imported from the navigation platform to the HIFU modeling environment for simulating the performance of a full conformal tumor ablation (**Fig. 4**). As a 1st approximation, the time of displacement of the robot, as encountered in a real experiment, was neglected and all t_{OFF} between single exposures were set to 0 s. As a 2nd approximation, the 3D conformal HIFU planning was designed while considering the performances of independent single HIFU exposure, the cumulative heat deposition effect arising in series of successive HIFU exposures was thus neglected. This approximation was considered acceptable with the HIFU exposure zig-zag trajectory which was expected to homogenize spatially any potential overtreatments. After the end of the simulation, 3D temperature and thermal dose maps were re-exported from the HIFU modeling environment to the virtual navigation environment and fused with target tumor segmentations for further analyses of the treatment conformation.

2.9 HIFU simulation model

HIFU simulations were used at 2 key moments in the presented study (HIFU pre-tuning and conformal HIFU treatments). In both cases, the same theoretical models, simulating tools and parameters were used. The ultrasound pressure fields were first computed using the Rayleigh surface integral for dynamic focusing depths ranging from 6 to 20 mm. The HIFU elements were simulated as homogeneous surfaces with piston like vibrations. The nonlinear propagation and cavitation effects were neglected in the calculations. Then, simulations were performed including attenuating tissues. The temperature increases induced by HIFU exposures in liver tissues were calculated using the Bio Heat Transfer Equation (BHTE)[59], and the resulting thermal ablations were estimated using the thermal dose model of equivalent time at 43 °C[60]. It is generally admitted that a thermal dose ≥ 240 CEM induces a complete cell death in liver tissue[61]–[63]. The environment around the interstitial HIFU prototype was simplified to 2 media (water for the cooling system at

the front of the transducer and homogenous liver tissues). The tissue physiological and physical parameters used for HIFU simulations are described in **Table 1**[64]. First, a sufficiently large attenuating medium > 100 mm was defined to mimic the presence of liver tissue (no ultrasound reflections considered). Second, a 3-mm in diameter cylindrical hole inserted at the center of the liver and filled with water mimicked the prototype cooling system placed at the front of the ultrasound transducer. Such system is commonly used experimentally to ensure the acoustic coupling between the HIFU transducer and the liver tissues, and to cool down the transducer during HIFU exposures. The ultrasound surface intensity output was adjusted to the maximum reachable with the dual-mode prototype, I_{ac} = 20 W.cm^{-2} (manufacturer data).

2.10 Assessment of results

For evaluating the 3D US image reconstruction, the image resolution was assessed by imaging a 70-µm in width copper wire and by measuring the width of its spatial impulse response at -6 dB (full-width at half maximum). Given that 3D US images were obtained by rotating the prototype around its insertion axis, a cylindrical coordinate system was used with its longitudinal axis coincident with the probe insertion axis. The image resolution was measured at a radial depth of 30 mm (r-axis). Since the prototype had a maximal treatment radius of 20 mm (preliminary HIFU simulations), this provided a 1-cm margin for imaging beyond the ablated tissues. The quality of the tumor-mimic visualization was quantified by measuring the contrast $C = \frac{S_{tumor}-S_{liver}}{S_{liver}}$, between the tumor-mimic mean signal S_{tumor} and the surrounding liver tissue mean signal S_{liver}. The accuracy of tumor volume estimation was evaluated by comparing 3D US-image based tumor-mimic segmentation volumes, V_{US}, to a reference volume, V_{ref}, measured by the water displacement method. For evaluating the 3D US-navigation guidance, all HIFU modeling investigations were analyzed as follows. The resulting ablated tissue volumes was defined using the 3D thermal dose field, t_{43} (x,y,z), obtained after the completion of the last HIFU exposure, and by considering all voxels with a thermal dose > 240 CEM. The treated volume (HIFU ablation) was overlaid and compared to the targeted volume (tumor-mimic). A Dice Similarity Coefficient (DSC) for volumetric comparisons was used as an indicator of the treatment conformation[65]. This coefficient was calculated as follows: $(V, V') = 2 \times \frac{V \cap V'}{V+V'}$, with respectively, V and V' the targeted volume (tumor-mimic) and the HIFU ablation volume (treatment). A DSC coefficient of 0 indicated that the 2 volumes were disjoint, while a coefficient of 1 indicated they were equals. DSC is particularly well suited for evaluating the accuracy of conformal thermal therapy because it not only penalizes volume differences between the

targeted and ablated regions, but also accounts for the presence of under- and over-treated regions[66]. Treatment time and targeting accuracy were analyzed with the following parameters: treatment time (min), treatment rate ($cm^3.min^{-1}$), ablated volume (cm^3), volumetric over- and under-treatment (cm^3 and %).

3 Results

3.1 Real-time data transfer for US navigation in tissues

The US-navigation station received a 2D US image of the *in-vitro* tissues every 100 ms (data stream #1), and a matrix representing the robot flange position in space every 50 ms (data stream #2). These communication rates allowed real-time 2D visualization of the tumor-mimic and surrounding liver tissues, as well as smooth real-time US navigation within the 3D virtual environment, as the prototype was moved by the robot. 3D US image reconstructions were then successfully obtained in the virtual space after robot-assisted scanning with 2D US images.

3.2 3D interstitial US imaging of tumor-mimics

Large tumor-mimics of various shapes were successfully created *in vitro*, especially ovoid- and disc-shaped tumors (**Fig. 5**). Overall, 8 in-vitro HCC tumor-mimic models were created. Their major diameters ranged from 42 to 23 mm, while their minor diameters ranged from 35 to 12 mm. The resolution of the 3D US image at a distance of 3 cm from the probe was 0.7 mm along r-axis, 5.8 mm along u_θ-axis and 1.7 mm along z-axis. Despite the resolution of several millimeters along u_θ-axis, 3D US images were successfully reconstructed interstitially and *in situ*. The obtained US image volumes allowed clear visualization of the 3D tumor-mimic shapes within liver tissues (**Fig. 6**). The virtual environment allowed successful 3D navigation within the US image volume. The operator had access to several useful information for further HIFU treatment guidance and planning, such as: i) real-time 2D B-mode images (**Fig. 6a**); ii) multi-planar and volumetric views of the 3D US imaging reconstruction allowing the operator to navigate through the US image volume, visualize the entire tumor site in 3D or in any 2D cross-sectional plans (**Fig. 6b-d**). All the trials summarized in **Table 2**. Depending on the tumor height (z-axis) and prototype insertion strategy (inside or beside the tumor), various sizes of US volumes were reconstructed to cover the entire tumor-mimic volumes. The minimum and maximum heights of the reconstructed US image volumes ranged 13-33 mm and 52-69 mm respectively. In case of insertion inside the tumor, a full 360°-rotation of the prototype was always performed for imaging and further HIFU treatment planning. However, in case of insertion beside the tumor, the prototype rotation could be significantly reduced

while achieving full tumor coverage, with imaging angular sector ranging, here, from 88 to 179°. Each tumor-mimic appeared as a homogenous region, hyperechoic when compared to the echogenicity of the surrounding liver tissues. The contrast measured between the 2 tissues, C = 1.7 ± 0.4 (range 2.3 - 1.1), allowed accurate manual segmentations of tumor-mimic volumes, plan by plan, using the reconstructed azimuthal 2D US images (xOy plan) (**Fig. 7a**). A 3D surface representing the 3D tumor boundaries was then automatically created by interpolations over all 2D azimuthal segmentations (**Fig. 7b-d**). The tumor-mimic volumes, V_{US} = 12 ± 9 cm^3 (range 3 - 30 cm^3), were accurately estimated from 3D US-image-based segmentations, when compared to the reference tumor volumes V_{ref} = 12 ± 9 cm^3 (range 3 - 29 cm^3).

3.3 Automatic conformal HIFU planning

Conformal HIFU treatment planning was automatically created by distributing focal points on the 3D tumor surface and by associating optimal HIFU exposure durations (pre-tuning simulation). Over all trials, the number of focal points necessary to cover a tumor-mimic entirely ranged from 93 to 1118, which corresponded on average to a density of focal points per unit tumor surface of 13 ± 5 focal points/cm^2. Given the tumor-mimic geometries studied, HIFU treatment planning included from 2 to 4 stages with angular apertures ranging from 67° to 360° in case of insertion inside the tumor-mimic mass. Minimum and maximum HIFU target distances were respectively of d_{min} = 10 ± 5 (range 5 - 20 mm) and d_{max} = 29 ± 7 (range 22 - 41 mm). **Figure 8a** shows an example of automatic focal point computation for a small segmented target adjacent to the probe (case #8). In this case, only 2 stages and 93 focal points were needed to treat the whole volume. In **figure 8b**, the probe was inserted inside the tumor (case #6). In this case, the probe had to perform a 360° rotation to treat the whole target. Four stages and 1118 focal points were then needed to treat this volume.

3.4 US-navigation guided HIFU ablations

The last module embedded in the HIFU treatment planning platform allowed estimating the final performances of a HIFU prototype in achieving successfully a given conformal treatment planning. All HIFU simulation results are reported in details in **Table 3**. In the 4 cases (1 to 4) where the treatment planning included target distances far beyond the prototype focusing capacities ($d_{max} \leq$ 41 mm), non-negligible undertreated volumes were quantitatively assessed for further re-evaluation of the treatment strategy. In all other cases, where the maximum target distances remained < 25 mm, a full conformal ablation of the tumor could be performed either from the inside or from the outside of the tumor (**Table 3**, see cases 5 to 8). In these

cases, the ablation volumes conformed precisely to the target tumor-mimic volumes with DSC ranging 0.6-0.9. Under- and over-treatments remained respectively < 0.1 cm^3 and < 9.5 cm^3. The total treatment time ranged from 14 to 124 min, for a treatment rate ranging from 0.3 to 0.4 cm^3/min. **Figure 9** shows the simulated thermal dose > 240 CEM obtained after the completion of the last HIFU exposure as seen in the visualization software. **Figure 9d** illustrates the case where the target volume was too far from the probe axis, with the consequence that some tumor tissues were not treated. In all cases, the 3D navigation platform enabled to overlay different data types (thermal dose and reconstructed 3D US volume) and to navigate in 3D between the different slices to assess the treatment result.

4 Discussion

4.1 A modular platform for studying conformal USgHIFU therapies

Conformal high intensity ultrasound therapies have already shown promise up to the clinical level for the minimally-invasive treatment of localized tumors[67]. To date however, the development of these emerging strategies always requires advanced systems (MRI) in order to deliver and guide the treatment. Few HIFU systems have been proposed so far to control conformal treatments in 3D in a standard MRI-free operative room. In the presented work, an advanced USgHIFU platform has been developed, which couples dual-mode US/HIFU technologies with emerging robotic and navigation techniques in medicine[68]–[71]. The platform allowed driving an interstitial dual-mode probe for in-situ volume imaging and 3D treatment planning, by combining together several research tools such as a Verasonics US scanner and a KUKA robotic arm. It is important to note that the architecture of this open research platform has been thought to be modular, and allows integrating any devices compliant with the OpenIGTLink data structure. This modularity makes it possible to use the tools developed (treatment planning and execution) for other research projects, with a minimum need for refactoring. For instance, in an ongoing work (unpublished yet), the robot-assisted US navigation platform is currently used with little modifications to drive an extracorporeal HIFU device, with different US scanner and power generator. This illustrates the flexibility offered by such research platforms for studying various US-guided HIFU approaches (not only interstitial). This modularity is especially due to the architecture of the visualization interfaces (3DSlicer and Plus Toolkit software). This architecture also allows the integration of other modalities which are interesting for image-guided treatment planning. For instance, optical or magnetic tracking methods are directly compatible for tracking the position in space of the probe, which

could be useful for applications where few focal points are needed and the use of a robotic arm is not relevant. Other types of image data can also be mixed in the 3D visualization environment. Here, only B-mode US images were involved, but other types of US-based images could be used, especially for the treatment monitoring phase. Although current US-based monitoring methods are not as consistent as MR thermometry, US elastography methods are promising and could be associated to measure tissues stiffness variation over time and assess the extent of the thermal lesion.

4.2 Developing interstitial 3D conformal USgHIFU therapies

In this study, 3 steps have been highlighted to achieve full conformal HIFU ablations using the proposed interstitial approach. The first 2 steps, including 3D US imaging reconstructions of target tumor volumes and conformal HIFU treatment planning strategies, were validated experimentally *in vitro*. Despite the small size of the prototype, the series of 2D B-mode images acquired enabled the reconstruction of 3D US image volumes which had sufficient quality to segment properly tumor-mimic inclusions. However, these in-vitro experiments were conducted in favorable conditions without tissue movement, as those due to respiratory activity during interstitial procedures in real clinical conditions. In case of tissue motion relative to the interstitial prototype during the reconstruction process, the reconstructed image volume would not be accurate anymore. To avoid this, High Frequency Jet Ventilation (HFJV) techniques can be used to properly ventilate patients without substantial movements of the rib cage[72] (residual movement: ~ 5 mm[73]). An alternative solution could consist in using the moment sensors of the robot, which theoretically allows computing and minimizing the mechanical load on the prototype after displacing it accordingly. US-image-based motion tracking method could also be proposed to estimate the global liver tissue displacement in real-time for mechanical motion compensation with the robot[74], [75]. This could be done, for instance, with the abdominal US imaging probe used conventionally in clinical procedures to guide the interstitial punctures.

The last step, related to treatment execution, has been validated in modeling with useful results for guiding future interstitial HIFU strategies. It has been confirmed that one major interest of using interstitial ultrasound compared to standard interstitial modalities was the ability to orientate the thermal ablation in specific directions and to preserve critical anatomical or functional structures. Such US navigation platform allowed planning this energy deposition conformally in 3D. The estimated treatment durations and ablation rates was then useful to highlight on which tumor shapes or locations a specific USgHIFU catheter should be

preferentially used, in terms of efficacy, accuracy and safety. In the procedure studied here, an automatic conformal HIFU treatment planning was proposed with encouraging results, while several aspects in the focal point determination could be further studied using the developed platform, especially to optimize the number and distribution of the focal points on the tumor 3D surface. For simulating conformal HIFU ablations, the spacing between focal points was adjusted to be of the order of magnitude of the HIFU focal region dimension, to ensure homogeneous thermal ablations within tumors. However, there is a tradeoff between the number of focal points required to ablate the entire tumor volume properly and the total treatment duration. Optimizing the HIFU energy deposition over the tumor 3D surface (focal point number, positions) is challenging but is crucial to ensure homogenous ablations while achieving reasonable treatment times.

For a 3-cm-diameter ovoid-shape tumor, the treatment durations reported here for conformal ablations with this 1st version of interstitial USgHIFU prototype (> 1 h), were rather long compared to current non-conformal Radio Frequency Ablation procedures in liver (~ 20-30 min)[76]. This suggests that this specific prototype design might not be optimal for treating these tumor geometries, unless the conformality of the ablation is mandatory in the case studied (e.g. a critical region to protect for the patient safety). In fact, treatment duration was drastically increased by the need to divide a treatment in several stages requiring device translations and repeating rotations. As a consequence, when only 1 treatment stage was needed, full conformal HIFU ablations were achievable much more rapidly, within 30-45 min. This specific prototype design then appeared to be optimal for treating disc-shape tumors with diameters > 30 mm, as soon as their height remained ≤ 13 mm (transducer height). Theoretically, modulating acoustic frequency may allow to efficiently deposit heat at different depths. Yet in CW mode, to avoid transducer damage due to overheating, transducer are standardly driven at their mechanical resonance frequencies, regardless of the tissue depth or type. Few studies have proposed to use either the third harmonic resonance frequency [77] or high impedance front layer [78], in order to drive transducers at several discrete frequencies optimized for different treatment depths. In both strategies, however, the electro-acoustic efficiency must remain high enough which depends on the transducer technologies. Otherwise, the advantages in heat deposition provided by the frequency modulation could be limited by the obligation to reduce the acoustic intensity in order to preserve the transducer integrity. Modulation of the acoustic intensity at the surface of the transducer is also interesting, especially to avoid boiling effects. However, given the transducer acoustic intensity limit (20 W.cm^{-2}) and its miniature surface

area (0.26 cm2), pre-tuning simulations have shown that temperature over 100°C should not be reached in the presented treatment configuration. Conformal HIFU treatment simulations also allowed estimating quantitatively the role of thermal diffusion in this particular interstitial configuration which, for the cases studied, helped reaching larger ablation radii. Homogenous thermal ablations were achieved over 24-mm radii despite application of HIFU for a shorter amount of time compare to single shot tuning simulations. Then, considering thermal diffusion effects in the treatment planning algorithm could also help reducing the total treatment duration. Instead of using a thermal dose abacus based on single independent HIFU exposures, pre-tuning simulations based on multiple HIFU exposures would contribute accounting for thermal diffusions from previous HIFU exposure contributions.

After considering the 3D guidance and planning, one remaining major challenge of interstitial conformal HIFU therapies may be related to the HIFU technology itself, and its ability to provide sufficient ultrasound energy. In the meantime, catheter miniaturization is a key point to compete with other techniques (RF, Cryo, Microwave ablations) and to provide the advantages associated to minimally-invasive procedures. Here, thermal lesions were obtained by assuming the ability to deliver robustly an acoustic intensity of 20 W/cm^2 at the surface of the transducers during several dozens of minutes in CW regime. In the literature, several studies have reported the ability to reach surface intensities ranging 10-40 W/cm^2 [34], [39], [79]. However, all these presented systems were larger than the dual-mode prototype involved in this study, and the literature is lacking data on the robustness of HIFU devices. Piezo technologies are associated with some thermal and mechanical damages which can be prevented in certain conditions (e.g. using cooling systems for reducing transducer self-heating). The design of the presented interstitial dual-mode prototype thus remains to be fully validated in HIFU mode, before achieving thermal ablations experimentally. In parallel to the standard in ultrasound transduction, recent works have also suggested the potential of emerging technologies coming from the MEMs domain, such as Capacitive Micromachined Ultrasound Transducers (CMUTs), to provide an alternative in the development of miniaturized image-guided HIFU systems [80]–[82]. All these aspects are critical to transfer new conformal therapeutic strategies into clinic. The presented US-navigation platform and conformal planning methodology are fully compatible with these emerging ultrasound technologies.

4.3 Computer-assisted HIFU modeling during USgHIFU interventions

In the presented work, simulations were only intended to validate that the developed automatic treatment planning strategy can effectively generate a conformal lesion. But simulations could also be useful intraoperatively, at the time of the HIFU treatment procedure, to help anticipating the treatment outcome. Improving HIFU simulation platforms would provide new tools to assist the interventional radiologist with predicting, in an early stage of the treatment, the possible thermal lesion shape. To date however, several challenges remain to be addressed for bringing HIFU simulation in an operative room. Such HIFU treatment simulations take several hours to complete, therefore they currently are too time consuming to be usable during an interventional procedure.

In its current state, computer simulations suffer not only from calculation duration limitation, but also from the limited accuracy of the physical models used. According to the literature, HIFU simulations often modeled liver tissues as a homogeneous and isotropic medium associated to constant thermal and acoustical characteristics. Although these standard approximations are commonly accepted to make decisions in the developments of HIFU devices and exposure strategies, these models may not be sufficiently precise to influence decisions at the time of interventions. Actual tissues are indeed much more complex as they have spatially heterogeneous physical parameters, which also evolve over time as the HIFU treatment modifies tissues properties. Non-linear effects, acoustic reflections, boiling and cavitation were not modeled neither, although some efforts have been made to avoid these phenomenon with appropriate choices in the ultrasound parameters. A homogeneous medium also means that the heat sink effect around large blood vessel was not modeled. The water cooling of the prototype was also modeled with several approximations, and did not consider water circulation, convection effects and the finite size of the water cooling window actually in contact with liver tissues, as the prototype was moved. These specificities were not considered since the main objective was to observe the thermal lesion extent, especially at the border of the tumor, to confirm the ability of the automatic treatment planning algorithm to create conformal thermal ablations. To date, HIFU computer simulations help considering order of magnitudes of the physical phenomena and highlighting trends while studying the effect of varying some treatment or tissue parameters. However, using simulations to assist a radiologist in the interventional decisions could require a higher level of precision of the physical models used. Especially, it is critical not to reach undesirable 100°C-temperatures associated with the appearance of boiling,

which creates acoustic barrier and diffusion affecting the dynamic of the temperature evolution in tissues. But to date, the knowledge of the precise thermal and acoustical tissue parameters remain challenging, since these parameters vary significantly from one individual to another, and their accurate measurements are either not trivial or simply not possible in realistic conditions.

In the presented study, the abacus built and used as a reference to determine HIFU exposure durations is based on mean physical parameters. Hence, the HIFU exposure durations selected for the conformal treatment planning may not be accurate for every tumor environment. Thus the conformation accuracy of the final ablated volume cannot yet be guaranteed for a given patient by using this abacus method only. To do so, new measurement methods will have to be available at the clinical level, in order to access personalized acoustic and physiological parameters *in vivo* and to refine the predictions of thermal ablations according to the individual characteristics of each patient. Hence, the development of novel real-time monitoring techniques remains critical to achieve efficient, accurate and safe conformal treatment. The platform developed in this work also perfectly aims to provide a common environment of communication between the modeling and monitoring tools, so that they can feed each other and better assist the intervention.

5 Conclusion

An original open research platform has been developed to promote the interest of US-image based navigation techniques coupled to robotic, in the development of interstitial 3D USgHIFU conformal therapies of localized tumors. The technical and methodological feasibilities have been demonstrated experimentally by validating, with a dual-mode USgHIFU catheter, the ability to perform US image volume reconstruction, 3D treatment planning of in-vitro liver tumor-mimics and conformal ablation predictions in a standard operative room. The platform also allowed confirming satisfying theoretical HIFU treatment performances for the conformal ablations of solid disc-shape tumors with the same catheter prototype. The architectural modularity of this US-navigation platform, making it compatible with various research medical devices, has the potential to provide a powerful research tool to study a broad range of image-guided HIFU procedures, and accelerate the development of conformal USgHIFU strategies at the preclinical and clinical level.

6 Acknowledgements

Authors are grateful to the 3DSlicer and Plus Toolkit communities for their help and reactivity on their different internet forums. This work has been founded by France Life Imaging (MUSTANG project, FLI, WP3, 2014), the French Public Investment Bank (HECAM project, BPI, PIA, PSPC 2015), the French Ministry of Higher Education and Research (MESR, EDISS 2016) and the French Laboratory of Excellence (labex) DevWeCan.

7 Author Contributions

L. D. designed the study, conducted the experiments, carried out the simulations, processed the raw data, analyzed the results and wrote the manuscript. A.N. and M.L.G. carried out the simulations and provided technical support. J.Y.C. reviewed the manuscript. W.A.N. designed the study, provided critical feedback for the different steps of this study, analyzed the results and reviewed the manuscript.

8 Conflicts of interests

The authors declare no conflict of interest.

9 Bibliography

[1] T. de Baere and F. Deschamps, “Treatment of hepatic and pulmonary metastases with radiofrequency,” *Diagn. Interv. Imaging*, vol. 95, no. 7–8, pp. 683–688, Jul. 2014, doi: 10.1016/j.diii.2014.04.017.

[2] R. Lencioni and L. Crocetti, “Radiofrequency Ablation of Liver Cancer,” *Tech. Vasc. Interv. Radiol.*, vol. 10, no. 1, pp. 38–46, Mar. 2007, doi: 10.1053/j.tvir.2007.08.006.

[3] T. de Baere and F. Deschamps, “New tumor ablation techniques for cancer treatment (microwave, electroporation),” *Diagn. Interv. Imaging*, vol. 95, no. 7–8, pp. 677–682, Jul. 2014, doi: 10.1016/j.diii.2014.04.001.

[4] C. Kim, “Understanding the nuances of microwave ablation for more accurate post-treatment assessment,” *Future Oncol.*, vol. 14, no. 17, pp. 1755–1764, Jul. 2018, doi: 10.2217/fon-2017-0736.

[5] D. Sindram, R. Z. Swan, K. N. Lau, I. H. McKillop, D. A. Iannitti, and J. B. Martinie, “Real-time three-dimensional guided ultrasound targeting system for microwave ablation of liver tumours: a human pilot study,” *HPB*, vol. 13, no. 3, pp. 185–191, Mar. 2011, doi: 10.1111/j.1477-2574.2010.00269.x.

[6] A. Carpentier *et al.*, “Real-time Magnetic Resonance-guided Laser Thermal Therapy for Focal Metastatic Brain Tumors,” *Oper. Neurosurg.*, vol. 63, no. suppl_1, pp. ONS21–ONS29, Jul. 2008, doi: 10.1227/01.NEU.0000311254.63848.72.

[7] Th. J. Vogl, R. Straub, S. Zangos, M. G. Mack, and K. Eichler, “MR-guided laser-induced thermotherapy (LITT) of liver tumours: experimental and clinical data,” *Int. J. Hyperthermia*, vol. 20, no. 7, pp. 713–724, Nov. 2004, doi: 10.1080/02656730400007212.

[8] H. W. Chen, E. C. H. Lai, Z. J. Zhen, W. Z. Cui, S. Liao, and W. Yee Lau, “Ultrasound-guided percutaneous cryotherapy of hepatocellular carcinoma,” *Int. J. Surg.*, vol. 9, no. 2, pp. 188–191, 2011, doi: 10.1016/j.ijsu.2010.11.008.

[9] Cheolkyun Kim, A. P. O’Rourke, D. M. Mahvi, and J. G. Webster, “Finite-Element Analysis of *Ex Vivo* and *In Vivo* Hepatic Cryoablation,” *IEEE Trans. Biomed. Eng.*, vol. 54, no. 7, pp. 1177–1185, Jul. 2007, doi: 10.1109/TBME.2006.889775.

[10] G. Deshazer, P. Prakash, D. Merck, and D. Haemmerich, “Experimental measurement of microwave ablation heating pattern and comparison to computer simulations,” *Int. J. Hyperthermia*, vol. 33, no. 1, pp. 74–82, Jan. 2017, doi: 10.1080/02656736.2016.1206630.

[11] M. K. Jain and P. D. Wolf, “A Three-Dimensional Finite Element Model of Radiofrequency Ablation with Blood Flow and its Experimental Validation,” *Ann. Biomed. Eng.*, vol. 28, no. 9, pp. 1075–1084, Sep. 2000, doi: 10.1114/1.1310219.

[12] G. Zorbas and T. Samaras, “Simulation of radiofrequency ablation in real human anatomy,” *Int. J. Hyperthermia*, vol. 30, no. 8, pp. 570–578, Dec. 2014, doi: 10.3109/02656736.2014.968639.

[13] S. E. Norred and J. A. Johnson, “Magnetic Resonance-Guided Laser Induced Thermal Therapy for Glioblastoma Multiforme: A Review,” *BioMed Res. Int.*, vol. 2014, pp. 1–9, 2014, doi: 10.1155/2014/761312.

[14] O. Ashraf, N. V. Patel, S. Hanft, and S. F. Danish, “Laser-Induced Thermal Therapy in Neuro-Oncology: A Review,” *World Neurosurg.*, vol. 112, pp. 166–177, Apr. 2018, doi: 10.1016/j.wneu.2018.01.123.

[15] J. G. Lynn, R. L. Zwemer, and A. J. Chick, “The Biological Application Of Focused Ultrasonics Waves,” *Science*, vol. 96, no. 2483, pp. 119–120, Jul. 1942, doi: 10.1126/science.96.2483.119.

[16] W. J. Fry, “Ultrasound in Neurology,” *Neurology*, vol. 6, pp. 693–704, 1956.

[17] W. J. Fry, W. H. Mosberg, J. W. Barnard, and F. J. Fry, “Production of Focal Destructive Lesions in the Central Nervous System With Ultrasound,” *J. Neurosurg.*, vol. 11, no. 5, pp. 471–478, Sep. 1954, doi: 10.3171/jns.1954.11.5.0471.

[18] J. E. Kennedy, “High-intensity focused ultrasound in the treatment of solid tumours,” *Nat. Rev. Cancer*, vol. 5, no. 4, pp. 321–327, Apr. 2005, doi: 10.1038/nrc1591.

[19] F. Aptel *et al.*, “Miniaturized High-Intensity Focused Ultrasound Device in Patients with Glaucoma: A Clinical Pilot Study,” *Investig. Opthalmology Vis. Sci.*, vol. 52, no. 12, pp. 8747–8753, Nov. 2011, doi: 10.1167/iovs.11-8137.

[20] R. Chopra *et al.*, “MR Imaging–controlled Transurethral Ultrasound Therapy for Conformal Treatment of Prostate Tissue: Initial Feasibility in Humans,” *Radiology*, vol. 265, no. 1, pp. 303–313, Oct. 2012, doi: 10.1148/radiol.12112263.

[21] S. Crouzet *et al.*, “Whole-gland Ablation of Localized Prostate Cancer with High-intensity Focused Ultrasound: Oncologic Outcomes and Morbidity in 1002 Patients,” *Eur. Urol.*, vol. 65, no. 5, pp. 907–914, May 2014, doi: 10.1016/j.eururo.2013.04.039.

[22] W. J. Elias *et al.*, “A Randomized Trial of Focused Ultrasound Thalamotomy for Essential Tremor,” *N. Engl. J. Med.*, vol. 375, no. 8, pp. 730–739, Aug. 2016, doi: 10.1056/NEJMoa1600159.

[23] W. J. Elias *et al.*, “A Pilot Study of Focused Ultrasound Thalamotomy for Essential Tremor,” *N. Engl. J. Med.*, vol. 369, no. 7, pp. 640–648, Aug. 2013, doi: 10.1056/NEJMoa1300962.

[24] F. M. Fennessy *et al.*, “Uterine Leiomyomas: MR Imaging–guided Focused Ultrasound Surgery—Results of Different Treatment Protocols [1],” *Radiology*, vol. 243, no. 3, pp. 885–893, Jun. 2007, doi: 10.1148/radiol.2433060267.

[25] A. Gelet *et al.*, “Transrectal High-Intensity Focused Ultrasound: Minimally Invasive Therapy of Localized Prostate Cancer,” *J. Endourol.*, vol. 14, no. 6, pp. 519–528, Aug. 2000, doi: 10.1089/end.2000.14.519.

[26] D. Gianfelice, A. Khiat, M. Amara, A. Belblidia, and Y. Boulanger, “MR Imaging–guided Focused US Ablation of Breast Cancer: Histopathologic Assessment of Effectiveness—Initial Experience,” *Radiology*, vol. 227, no. 3, pp. 849–855, Jun. 2003, doi: 10.1148/radiol.2281012163.

[27] N. Lipsman *et al.*, “MR-guided focused ultrasound thalamotomy for essential tremor: a proof-of-concept study,” *Lancet Neurol.*, vol. 12, no. 5, pp. 462–468, May 2013, doi: 10.1016/S1474-4422(13)70048-6.

[28] F. Wu *et al.*, “Extracorporeal focused ultrasound surgery for treatment of human solid carcinomas: early Chinese clinical experience,” *Ultrasound Med. Biol.*, vol. 30, no. 2, pp. 245–260, Feb. 2004, doi: 10.1016/j.ultrasmedbio.2003.10.010.

[29] R. Ritchie, J. Collin, C. Coussios, and T. Leslie, “Attenuation and De-focusing During High-Intensity Focused Ultrasound Therapy Through Peri-nephric Fat,” *Ultrasound Med. Biol.*, vol. 39, no. 10, pp. 1785–1793, Oct. 2013, doi: 10.1016/j.ultrasmedbio.2013.04.010.

[30] P. Gélat, G. ter Haar, and N. Saffari, “Modelling of the acoustic field of a multi-element HIFU array scattered by human ribs,” *Phys. Med. Biol.*, vol. 56, no. 17, pp. 5553–5581, Sep. 2011, doi: 10.1088/0031-9155/56/17/007.

[31] A. Dupré *et al.*, “First Clinical Experience of Intra-Operative High Intensity Focused Ultrasound in Patients with Colorectal Liver Metastases: A Phase I-IIa Study,” *PLOS ONE*, vol. 10, no. 2, p. e0118212, Feb. 2015, doi: 10.1371/journal.pone.0118212.

[32] C. Lafon, D. Melodelima, R. Salomir, and J. Y. Chapelon, “Interstitial devices for minimally invasive thermal ablation by high-intensity ultrasound,” *Int. J. Hyperthermia*, vol. 23, no. 2, pp. 153–163, Jan. 2007, doi: 10.1080/02656730601173029.

[33] V. A. Salgaonkar and C. J. Diederich, “Catheter-based ultrasound technology for image-guided thermal therapy: Current technology and applications,” *Int. J. Hyperthermia*, vol. 31, no. 2, pp. 203–215, Feb. 2015, doi: 10.3109/02656736.2015.1006269.

[34] R. Chopra, C. Luginbuhl, A. J. Weymouth, F. S. Foster, and M. J. Bronskill, “Interstitial ultrasound heating applicator for MR-guided thermal therapy,” *Phys. Med. Biol.*, vol. 46, pp. 3133–3145, Nov. 2001, doi: 10.1088/0031-9155/46/12/305.

[35] C. J. Diederich and E. C. Burdette, “Transurethral ultrasound array for prostate thermal therapy: initial studies,” *IEEE Trans. Ultrason. Ferroelectr. Freq. Control*, vol. 43, no. 6, pp. 1011–1022, Nov. 1996, doi: 10.1109/58.542046.

[36] G. Ghoshal *et al.*, “A minimally invasive catheter-based ultrasound technology for therapeutic interventions in brain: initial preclinical studies,” *Neurosurg. Focus*, vol. 44, no. 2, p. E13, Feb. 2018, doi: 10.3171/2017.11.FOCUS17631.

[37] C. Lafon, Y. Theillére, F. Prat, A. Arefiev, J. Y. Chapelon, and D. Cathignol, "Development of an interstitial ultrasound applicator for endoscopic procedures: animal experimentation," *Ultrasound Med. Biol.*, vol. 26, no. 4, pp. 669–675, May 2000, doi: 10.1016/S0301-5629(99)00157-X.

[38] W. Kwiecinski *et al.*, "Validation of an intracardiac ultrasonic therapy–imaging dual mode transducer," *IRBM*, vol. 36, no. 6, pp. 351–354, Nov. 2015, doi: 10.1016/j.irbm.2015.04.002.

[39] I. R. S. Makin, T. D. Mast, W. Faidi, M. M. Runk, P. G. Barthe, and M. H. Slayton, "Miniaturized ultrasound arrays for interstitial ablation and imaging," *Ultrasound Med. Biol.*, vol. 31, no. 11, pp. 1539–1550, Nov. 2005, doi: 10.1016/j.ultrasmedbio.2005.07.008.

[40] T. D. Mast *et al.*, "Treatment of Rabbit Liver Cancer In Vivo Using Miniaturized Image-Ablate Ultrasound Arrays," *Ultrasound Med. Biol.*, vol. 37, no. 10, pp. 1609–1621, Oct. 2011, doi: 10.1016/j.ultrasmedbio.2011.05.850.

[41] E. S. Ebbini and G. Ter Haar, "Ultrasound-guided therapeutic focused ultrasound: Current status and future directions," *Int. J. Hyperthermia*, vol. 31, no. 2, pp. 77–89, Feb. 2015, doi: 10.3109/02656736.2014.995238.

[42] S. Ellis, V. Rieke, M. Kohi, and A. C. Westphalen, "Clinical applications for magnetic resonance guided high intensity focused ultrasound (MRgHIFU): Present and future: Clinical applications for MRgHIFU," *J. Med. Imaging Radiat. Oncol.*, vol. 57, no. 4, pp. 391–399, Aug. 2013, doi: 10.1111/1754-9485.12085.

[43] C. M. C. Tempany, E. A. Stewart, N. McDannold, B. J. Quade, F. A. Jolesz, and K. Hynynen, "MR Imaging–guided Focused Ultrasound Surgery of Uterine Leiomyomas: A Feasibility Study," *Radiology*, vol. 226, no. 3, pp. 897–905, Mar. 2003, doi: 10.1148/radiol.2271020395.

[44] W. A. N'Djin *et al.*, "Active MR-temperature feedback control of dynamic interstitial ultrasound therapy in brain: *In vivo* experiments and modeling in native and coagulated tissues: MRT-controlled dynamic interstitial ultrasound brain therapy," *Med. Phys.*, vol. 41, no. 9, p. 093301, Aug. 2014, doi: 10.1118/1.4892923.

[45] B. Quesson, J. A. de Zwart, and C. T. W. Moonen, "Magnetic resonance temperature imaging for guidance of thermotherapy," *J. Magn. Reson. Imaging*, vol. 12, pp. 525–533, 2000, doi: 10.1002/1522-2586(200010)12:4<525::aid-jmri3>3.0.co;2-v.

[46] S. Vaezy *et al.*, “Real-time visualization of high-intensity focused ultrasound treatment using ultrasound imaging,” *Ultrasound Med. Biol.*, vol. 27, no. 1, pp. 33–42, Jan. 2001, doi: 10.1016/S0301-5629(00)00279-9.

[47] R. M. Arthur, W. L. Straube, J. D. Starman, and E. G. Moros, “Noninvasive temperature estimation based on the energy of backscattered ultrasound,” *Med. Phys.*, vol. 30, no. 6, pp. 1021–1029, May 2003, doi: 10.1118/1.1570373.

[48] J. Civale *et al.*, “Calibration of Ultrasound Backscatter Temperature Imaging for High-Intensity Focused Ultrasound Treatment Planning,” *Ultrasound Med. Biol.*, vol. 39, no. 9, pp. 1596–1612, Sep. 2013, doi: 10.1016/j.ultrasmedbio.2013.04.001.

[49] F. Kallel, R. J. Stafford, R. E. Price, R. Righetti, J. Ophir, and J. D. Hazle, “The feasibility of elastographic visualization of HIFU-induced thermal lesions in soft tissues,” *Ultrasound Med. Biol.*, vol. 25, no. 4, pp. 641–647, May 1999, doi: 10.1016/S0301-5629(98)00184-7.

[50] G. Bouchoux, C. Lafon, R. Berriet, J. Y. Chapelon, G. Fleury, and D. Cathignol, “Dual-Mode Ultrasound Transducer for Image-Guided Interstitial Thermal Therapy,” *Ultrasound Med. Biol.*, vol. 34, no. 4, pp. 607–616, Apr. 2008, doi: 10.1016/j.ultrasmedbio.2007.09.011.

[51] N. R. Owen *et al.*, “*In Vivo* Evaluation of a Mechanically Oscillating Dual-Mode Applicator for Ultrasound Imaging and Thermal Ablation,” *IEEE Trans. Biomed. Eng.*, vol. 57, no. 1, pp. 80–92, Jan. 2010, doi: 10.1109/TBME.2009.2023994.

[52] A. Fedorov *et al.*, “3D Slicer as an image computing platform for the Quantitative Imaging Network,” *Magn. Reson. Imaging*, vol. 30, no. 9, pp. 1323–1341, Nov. 2012, doi: 10.1016/j.mri.2012.05.001.

[53] A. Lasso, T. Heffter, A. Rankin, C. Pinter, T. Ungi, and G. Fichtinger, “PLUS: Open-Source Toolkit for Ultrasound-Guided Intervention Systems,” *IEEE Trans. Biomed. Eng.*, vol. 61, no. 10, pp. 2527–2537, Oct. 2014, doi: 10.1109/TBME.2014.2322864.

[54] F. Chavrier, J. Y. Chapelon, A. Gelet, and D. Cathignol, “Modeling of high-intensity focused ultrasound-induced lesions in the presence of cavitation bubbles,” *J. Acoust. Soc. Am.*, vol. 108, no. 1, pp. 432–440, Jul. 2000, doi: 10.1121/1.429476.

[55] J. Tokuda *et al.*, “OpenIGTLink: an open network protocol for image-guided therapy environment,” *Int. J. Med. Robot.*, vol. 5, no. 4, pp. 423–434, Dec. 2009, doi: 10.1002/rcs.274.

[56] W. A. N'Djin, D. Melodelima, H. Parmentier, M. Rivoire, and J. Y. Chapelon, "*In vivo* preclinical evaluation of the accuracy of toroidal-shaped HIFU treatments using a tumor-mimic model," *Phys. Med. Biol.*, vol. 55, no. 8, pp. 2137–2154, Apr. 2010, doi: 10.1088/0031-9155/55/8/002.

[57] W. A. N'Djin, D. Melodelima, H. Parmentier, S. Chesnais, M. Rivoire, and J. Y. Chapelon, "Utility of a Tumor-Mimic Model for the Evaluation of the Accuracy of HIFU Treatments. Results of In Vitro Experiments in the Liver," *Ultrasound Med. Biol.*, vol. 34, no. 12, pp. 1934–1943, Dec. 2008, doi: 10.1016/j.ultrasmedbio.2008.04.012.

[58] D. Scott *et al.*, "Development of an in vivo tumor-mimic model for learning radiofrequency ablation," *J. Gastrointest. Surg.*, vol. 4, no. 6, pp. 620–625, Dec. 2000, doi: 10.1016/S1091-255X(00)80112-2.

[59] H. H. Pennes, "Analysis of Tissue and Arterid Blood Temperatwes," *J. Appl. Physiol.*, vol. 1, no. 2, pp. 93–122, Aug. 1948, doi: 10.1152/jappl.1948.1.2.93.

[60] S. A. Sapareto and W. C. Dewey, "Thermal dose determination in cancer therapy," *Int. J. Radiat. Oncol.*, vol. 10, no. 6, pp. 787–800, Apr. 1984, doi: 10.1016/0360-3016(84)90379-1.

[61] M. R. Bailey, V. A. Khokhlova, O. A. Sapozhnikov, S. G. Kargl, and L. A. Crum, "Physical mechanisms of the therapeutic effect of ultrasound (a review)," *Acoust. Phys.*, vol. 49, no. 4, pp. 369–388, Jul. 2003, doi: 10.1134/1.1591291.

[62] C. Damianou and K. Hynynen, "The effect of various physical parameters on the size and shape of necrosed tissue volume during ultrasound surgery," *J. Acoust. Soc. Am.*, vol. 95, no. 3, pp. 1641–1649, Mar. 1994, doi: 10.1121/1.408550.

[63] N. J. McDannold, R. L. King, F. A. Jolesz, and K. H. Hynynen, "Usefulness of MR Imaging-Derived Thermometry and Dosimetry in Determining the Threshold for Tissue Damage Induced by Thermal Surgery in Rabbits," *Radiology*, vol. 216, no. 2, pp. 517–523, Aug. 2000, doi: 10.1148/radiology.216.2.r00au42517.

[64] F. A. Duck, *Physical properties of tissue: a comprehensive reference book.*, London: Academic Press. 1990.

[65] L. R. Dice, "Measures of the Amount of Ecologic Association Between Species," *Ecology*, vol. 26, no. 3, pp. 297–302, Jul. 1945, doi: 10.2307/1932409.

[66] J. P. Yung *et al.*, "Quantitative comparison of thermal dose models in normal canine brain: Quantitative comparison of thermal dose models in brain," *Med. Phys.*, vol. 37, no. 10, pp. 5313–5321, Sep. 2010, doi: 10.1118/1.3490085.

[67] J. L. Chin *et al.*, “Magnetic Resonance Imaging–Guided Transurethral Ultrasound Ablation of Prostate Tissue in Patients with Localized Prostate Cancer: A Prospective Phase 1 Clinical Trial,” *Eur. Urol.*, vol. 70, no. 3, pp. 447–455, Sep. 2016, doi: 10.1016/j.eururo.2015.12.029.

[68] G. Ameri *et al.*, “Development and Evaluation of an Augmented Reality Ultrasound Guidance System for Spinal Anesthesia: Preliminary Results,” *Ultrasound Med. Biol.*, vol. 45, no. 10, pp. 2736–2746, Oct. 2019, doi: 10.1016/j.ultrasmedbio.2019.04.026.

[69] M. Hastenteufel, S. Yang, C. Christoph, M. Vetter, H.-P. Meinzer, and I. Wolf, “Ultrasound-based navigation for minimally invasive surgical atrial fibrillation treatment: workflow and application prototype,” San Diego, CA, Apr. 2005, p. 400, doi: 10.1117/12.595203.

[70] F. Preiswerk, S. T. Brinker, N. J. McDannold, and T. Y. Mariano, “Open-source neuronavigation for multimodal non-invasive brain stimulation using 3D Slicer,” *ArXiv190912458 Physicsmed-Ph*, Sep. 2019, Accessed: Mar. 11, 2020. [Online]. Available: http://arxiv.org/abs/1909.12458.

[71] L. Yang *et al.*, “Vision-based endoscope tracking for 3D ultrasound image-guided surgical navigation,” *Comput. Med. Imaging Graph.*, vol. 40, pp. 205–216, Mar. 2015, doi: 10.1016/j.compmedimag.2014.09.003.

[72] J. Engstrand, G. Toporek, P. Harbut, E. Jonas, H. Nilsson, and J. Freedman, “Stereotactic CT-Guided Percutaneous Microwave Ablation of Liver Tumors With the Use of High-Frequency Jet Ventilation: An Accuracy and Procedural Safety Study,” *Am. J. Roentgenol.*, vol. 208, no. 1, pp. 193–200, Jan. 2017, doi: 10.2214/AJR.15.15803.

[73] P. Biro, D. R. Spahn, and T. Pfammatter, “High-frequency jet ventilation for minimizing breathing-related liver motion during percutaneous radiofrequency ablation of multiple hepatic tumours,” *Br. J. Anaesth.*, vol. 102, no. 5, pp. 650–653, May 2009, doi: 10.1093/bja/aep051.

[74] E. J. Harris, N. R. Miller, J. C. Bamber, J. R. N. Symonds-Tayler, and P. M. Evans, “Speckle tracking in a phantom and feature-based tracking in liver in the presence of respiratory motion using 4D ultrasound,” *Phys. Med. Biol.*, vol. 55, no. 12, pp. 3363–3380, Jun. 2010, doi: 10.1088/0031-9155/55/12/007.

[75] W. A. N’Djin, J.-Y. Chapelon, and D. Melodelima, “An Ultrasound Image-Based Dynamic Fusion Modeling Method for Predicting the Quantitative Impact of In Vivo Liver Motion on Intraoperative HIFU Therapies: Investigations in a Porcine Model,” *PLOS ONE*, vol. 10, no. 9, p. e0137317, Sep. 2015, doi: 10.1371/journal.pone.0137317.

[76] R. T. Poon *et al.*, “Learning Curve for Radiofrequency Ablation of Liver Tumors: Prospective Analysis of Initial 100 Patients in a Tertiary Institution,” *Ann. Surg.*, vol. 239, no. 4, pp. 441–449, Apr. 2004, doi: 10.1097/01.sla.0000118565.21298.0a.

[77] W. A. N’Djin, M. Burtnyk, M. Bronskill, and R. Chopra, “Investigation of power and frequency for 3D conformal MRI-controlled transurethral ultrasound therapy with a dual frequency multi-element transducer,” *Int. J. Hyperthermia*, vol. 28, no. 1, pp. 87–104, Feb. 2012, doi: 10.3109/02656736.2011.622343.

[78] R. Chopra, C. Luginbuhl, F. S. Foster, and M. J. Bronskill, “Multifrequency ultrasound transducers for conformal interstitial thermal therapy,” *IEEE Trans. Ultrason. Ferroelectr. Freq. Control*, vol. 50, no. 7, pp. 881–889, Jul. 2003, doi: 10.1109/TUFFC.2003.1214507.

[79] C. Lafon *et al.*, “Cylindrical thermal coagulation necrosis using an interstitial applicator with a plane ultrasonic transducer: in vitro and in vivo experiments versus computer simulations,” *Int. J. Hyperthermia*, vol. 16, no. 6, pp. 508–522, Jan. 2000, doi: 10.1080/02656730050199359.

[80] C. R. Bawiec, W. A. N’Djin, G. Bouchoux, N. Sénégond, N. Guillen, and J.-Y. Chapelon, “Preliminary Investigation of a 64-element Capacitive Micromachined Ultrasound Transducer (CMUT) Annular Array Designed for High Intensity Focused Ultrasound (HIFU),” *IRBM*, vol. 39, no. 5, pp. 295–306, Nov. 2018, doi: 10.1016/j.irbm.2018.09.001.

[81] W. A. N’Djin *et al.*, “Capacitive Micromachined Ultrasound Transducers for Interstitial High-Intensity Ultrasound Therapies,” *IEEE Trans. Ultrason. Ferroelectr. Freq. Control*, vol. 64, no. 8, pp. 1245–1260, Aug. 2017, doi: 10.1109/TUFFC.2017.2707663.

[82] H.-S. Yoon *et al.*, “Ex Vivo HIFU Experiments Using a 32 x 32 -Element CMUT Array,” *IEEE Trans. Ultrason. Ferroelectr. Freq. Control*, vol. 63, no. 12, pp. 2150–2158, Dec. 2016, doi: 10.1109/TUFFC.2016.2606126.

10 Figures and tables

(Please note that color should be used for all figures)

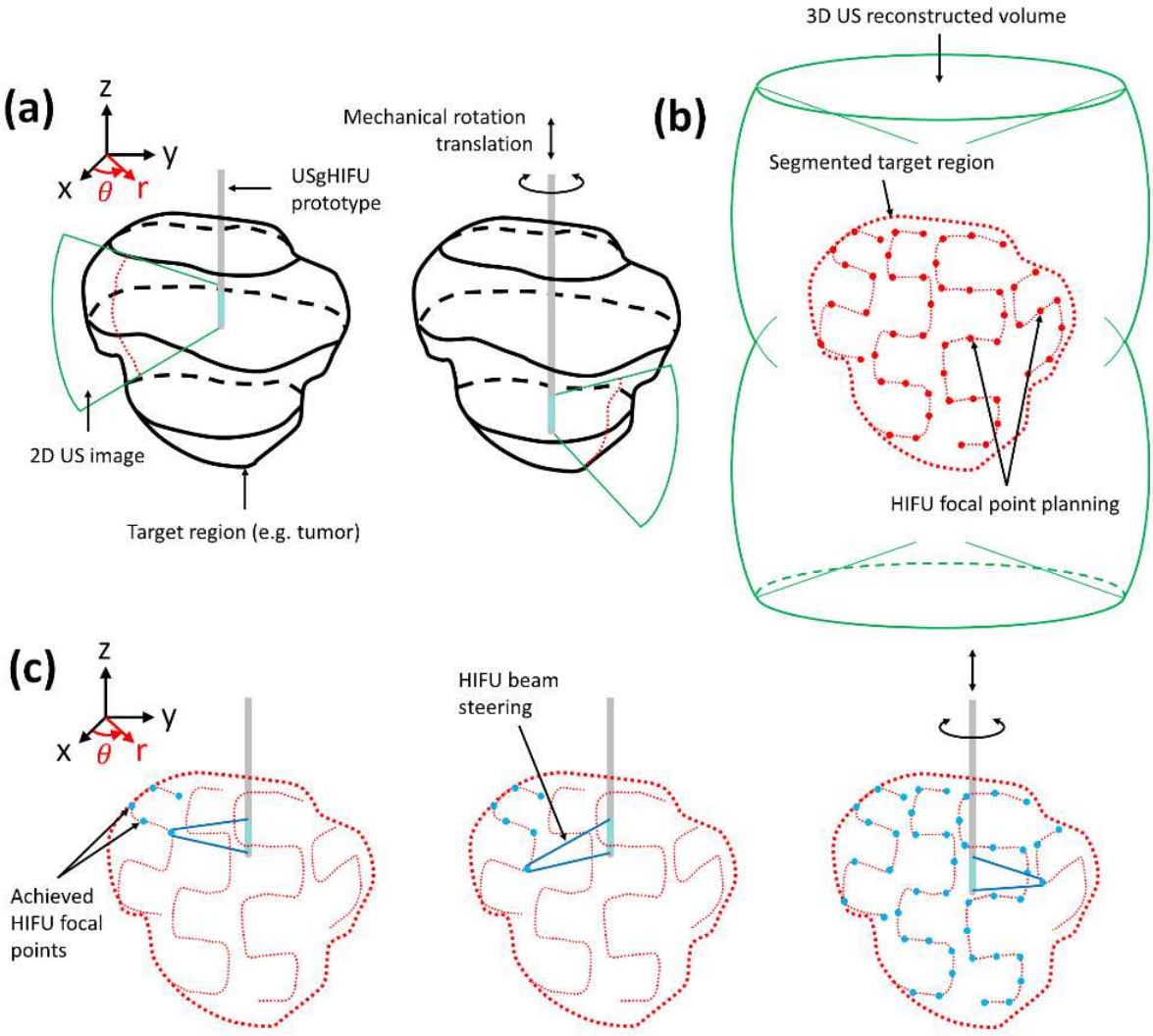

Fig. 1. 3D US-guided Navigation for interstitial conformal HIFU treatment planning: principle. (**a**) In-situ 3D US image reconstruction. A robot-assisted dual-mode USgHIFU interstitial prototype providing 2D sectorial B-mode US images was rotated and translated to image the entire volume of a target region *in situ* (e.g. from the inside of a tumor). (**b**) Target region segmentation and automatic determination of the focal points for covering the target region. (**c**) Conformal HIFU treatment. The dual-mode USgHIFU interstitial prototype provides 2D HIFU exposures with dynamic focusing capability. Robotic assistance allowed rotating and translating the prototype to ablate the entire volume of the target region interstitially.

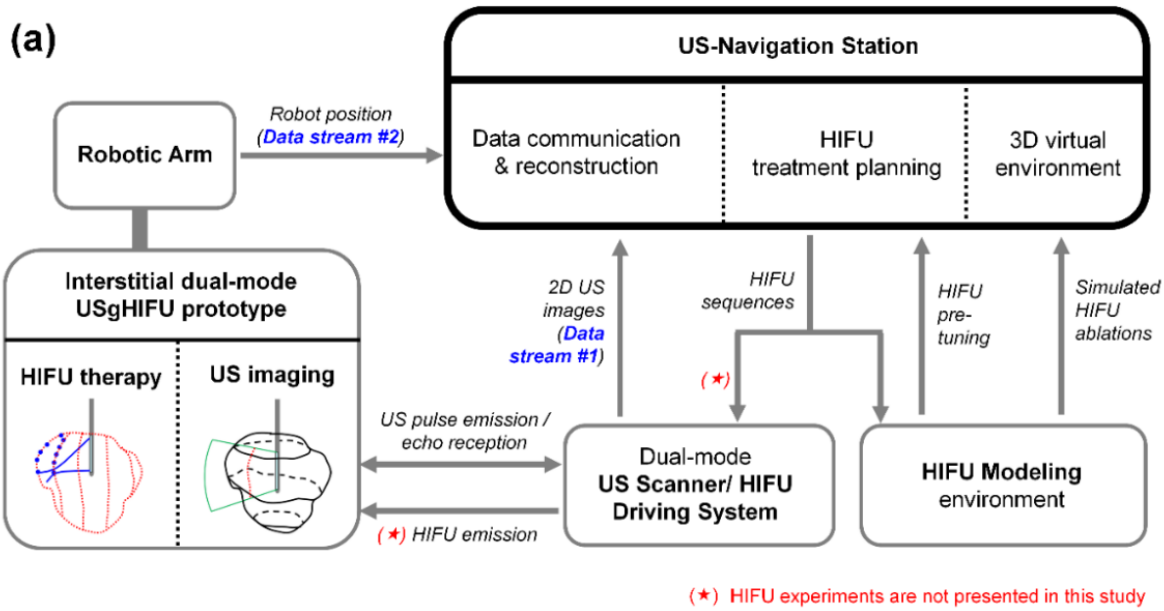

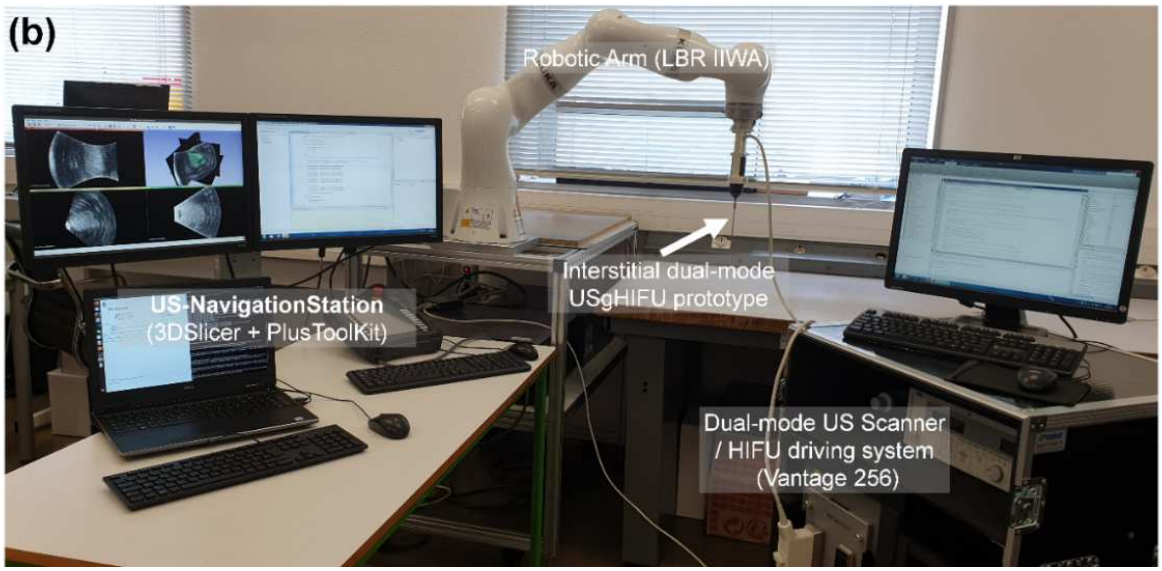

Fig. 2. Robot-assisted US-image based Navigation Platform for USgHIFU therapy. (**a**) Schematic diagram of the communication logic between each component of the platform. (**b**) Picture of the open research experimental platform.

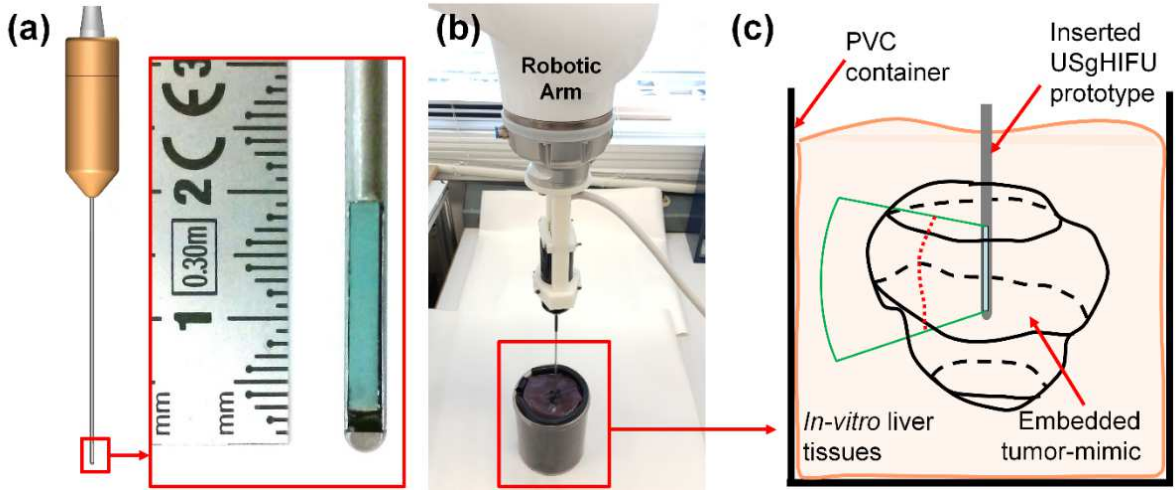

Fig. 3. In-situ interstitial 3D US imaging of tumor-mimic volumes in in-vitro liver tissues. (**a**) Interstitial USgHIFU prototype. (**b**) Picture of the experimental set-up: the robot-assisted USgHIFU prototype is inserted in a tumor-mimic agarose-based gel phantom, surrounded by in-vitro heifer liver. The ability of the reconstruction algorithm to generate 3D US image volumes of tissues has been tested on those phantoms. (**c**) Schematic view of the experimental US imaging set-up: zoom in on the mixed phantom/liver tissue sample.

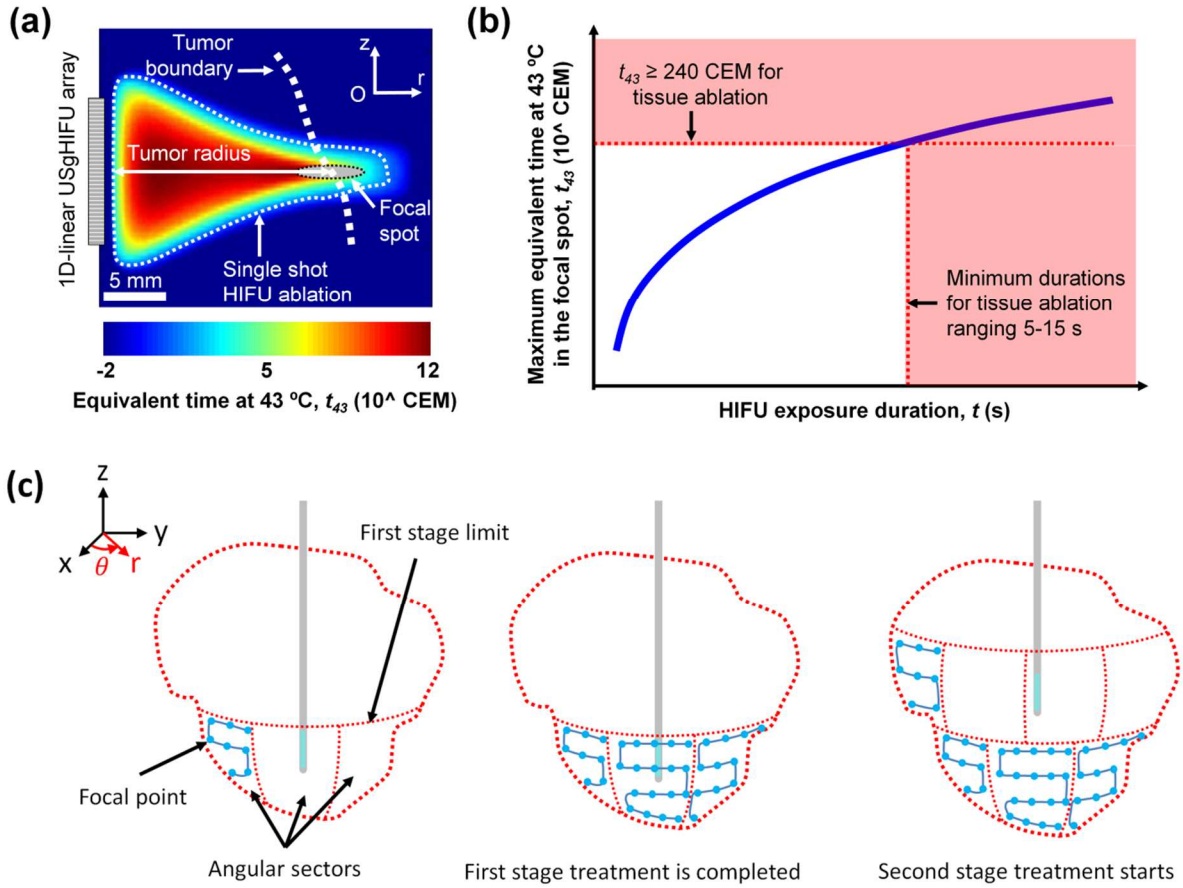

Fig. 4. Preliminary tuning in simulation of single HIFU exposures for 3D conformal HIFU treatment planning. (**a**) Simulated ablated area after a 15-s HIFU exposure dynamically focused (20-mm distance; 0-mm steering) to target a tumor boundary. The triangle-shaped ablation (t_{43} ≥ 240 CEM) allowed treating homogenously the whole tumor radius. (**b**) t_{43} (r, z, t) abacus were created to determine the minimum exposure duration t required to achieve homogenous ablations in all configurations of HIFU targeting determined for the 3D conformal treatment planning of a tumor. The exposure duration parameter was added to the spatial parameters obtained from the 3D tumor surface segmentation and the known relative position of the interstitial device. (**c**) HIFU trajectory: zig –zag strategy to optimize the heat deposition distribution.

Model component	Thermal conductivity (W/m/°C)	Specific heat (J/kg/°C)	Temperature (°C)	Perfusion ($kg/m^3/s$)	Density (kg/m^3)	Acoustic attenuation $A = a \cdot f^b$ (dB/cm/MHz)	Speed of sound (m/s)
Water (HIFU prototype cooling system)	0.627	4188	20	-	1000	a=0	1483
Liver	0.512	3600	37	18	1050	a = 0.4; b = 1.14	1578

Table 1: Tissue physiological and physical parameters used during numerical modeling of HIFU treatment in liver.

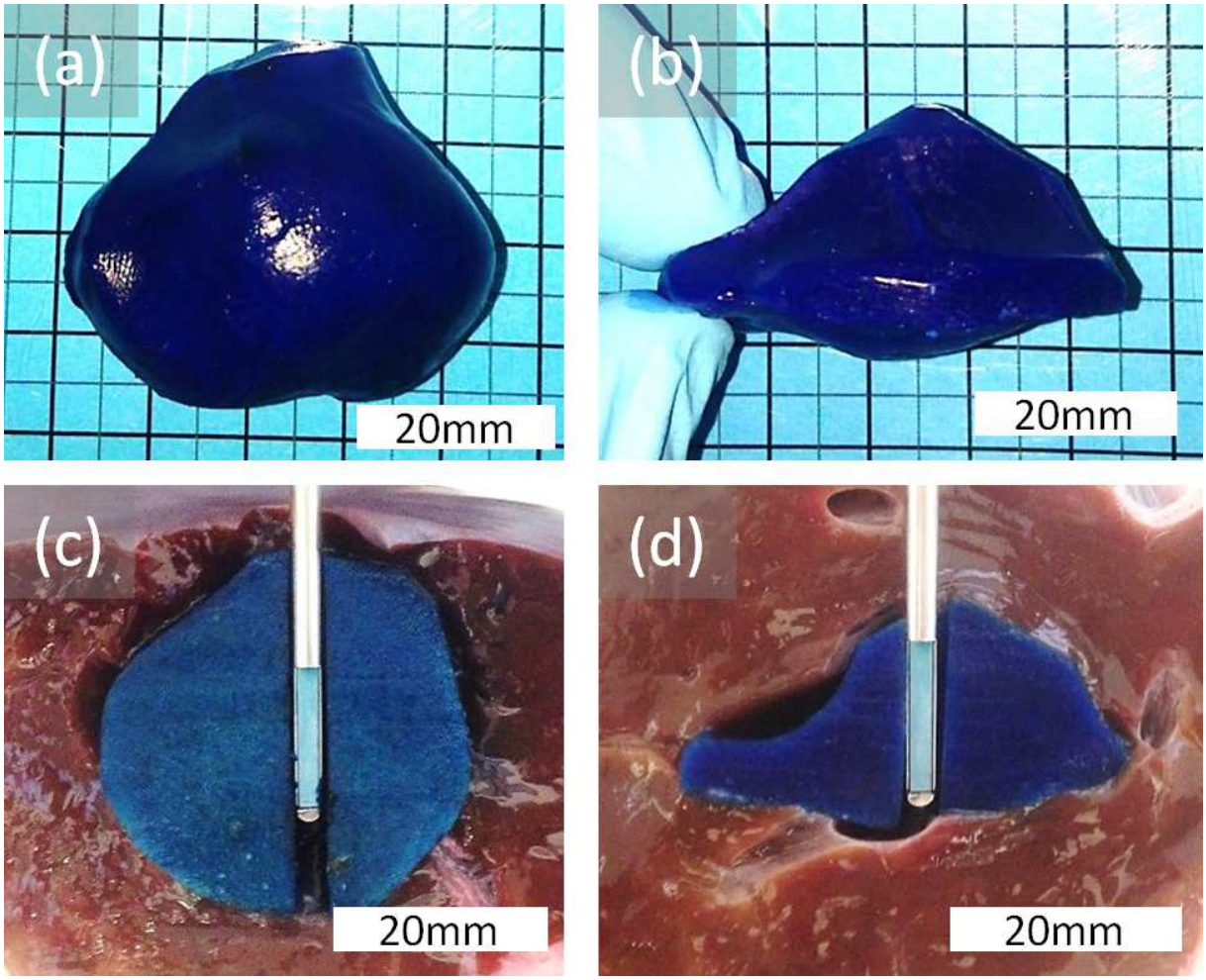

Fig. 5. In-vitro hepatocellular carcinoma tumor-mimic models obtained using soft molds. (**a**, **c**) Ovoid-shaped tumor-mimic gel, 41-mm in diameter and 35-mm in elevation. (tumor-mimic #6) (**b**, **d**) Disc-shaped tumor-mimic gel, 42-mm in diameter and 22-mm in elevation. (tumor-mimic #7)

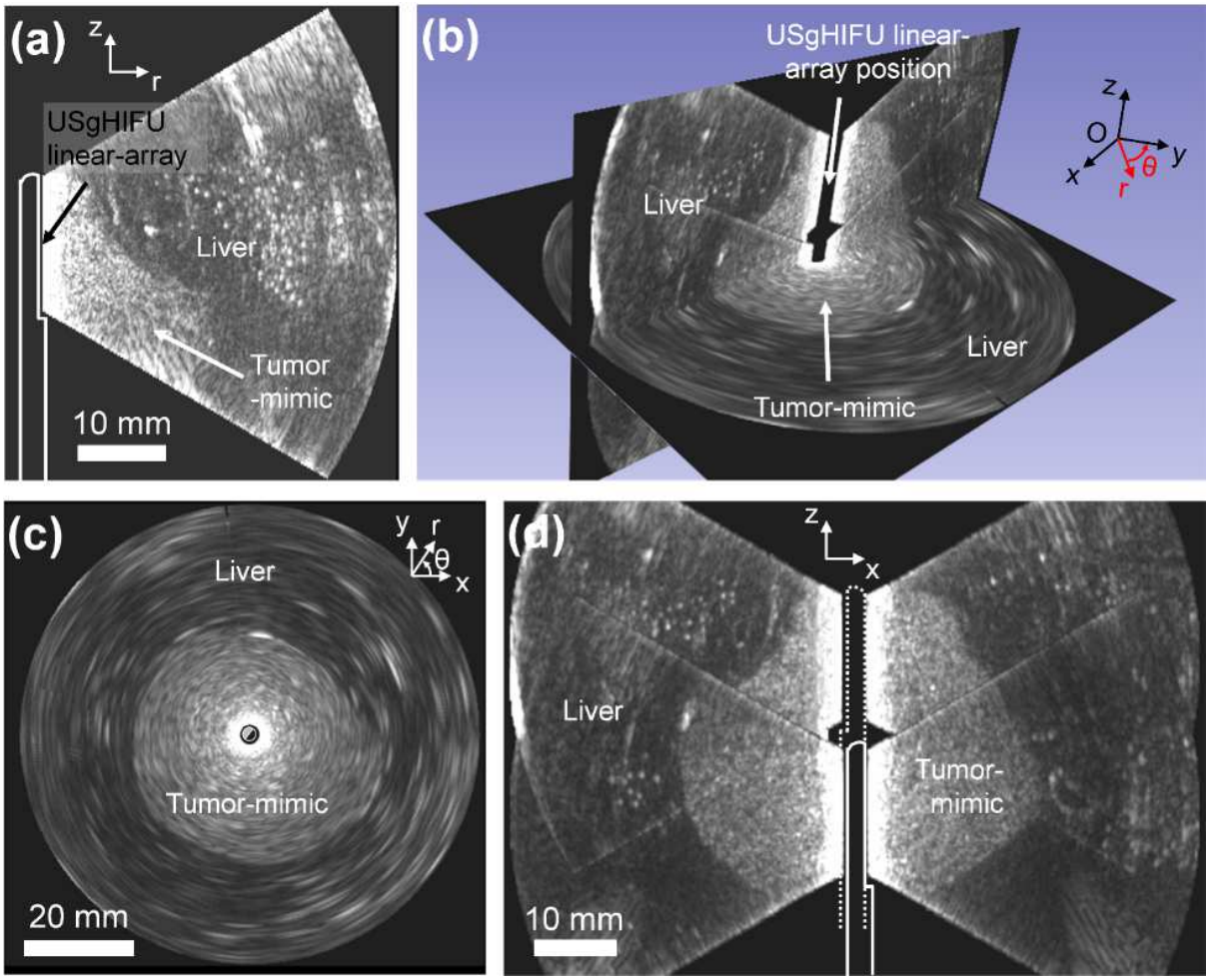

Fig. 6. In-situ 3D US imaging reconstruction, visualization and navigation in a tumor-mimic volume inserted in in-vitro liver tissues. Example where the USgHIFU prototype was inserted inside the tumor-mimic model (case #6). Two 360°-rotations were necessary to scan the whole tumor. (**a**) Real-time 2D B-mode image generated by the US scanner. (**b**) Multi-planar view of the 3D US imaging reconstruction after translation and rotation of the USgHIFU prototype. (**c**) Azimutal view reconstructed after rotation of the prototype (θ = 360°). (**d**) Elevational view reconstructed after 1 translation of the prototype (2 positions: $\Delta z = 18$ mm). The overlap between the 2 stages of sectorial images could be distinguished.

Tumor-mimic #	Interstitial prototype insertion	Reconstructed 3D US image			Tumor analysis on the 3D US image			Reference values (water displacement)	
		Angular sector/ prototype rotation, θ (°)	Radius (mm)	Height, h_{min}/h_{max} (mm), (Number of stage/prototype translation)	HIFU target distance, d_{min}/d_{max} (mm)	Prototype to tumor angular aperture (°)	Tumor-mimic volume, V_{US} (cm^3)	Tumor-mimic volume, V_{ref} (cm^3)	Volume relative difference $\frac{\lvert V_{US}-V_{ref}\rvert}{V_{ref}}$ (mean = 0.04)
1	Beside the tumor	167	50	13/61 (1)	8.2 / 29.8	154.1	9.6	9.6	0
2	″	119	50	13/61 (1)	11.3 / 36.1	89	8.6	8.5	0.01
3	″	88	50	13/61 (1)	19.4 / 40.7	67	8.4	7.8	0.08
4	″	118	50	13/61 (1)	13.5 / 32.1	94	7.6	6.6	0.15
5	Inside the tumor	360	40	33/69 (2)	5.0 / 22.6	360	20.6	21.3	0.03
6	″	360	40	33/69 (2)	6.2 / 24.3	360	29.7	28.5	0.04
7	″	360	40	13/52 (1)	5.0 / 21.9	360	10.2	10.1	0.01
8	Beside the tumor	179	40	13/52 (1)	7.6 /21.6	117	2.6	2.6	0

Table 2: Interstitial 3D US image reconstruction of tumor-mimic volumes in various configurations of device insertion: beside or inside the tumors. Summary of the image reconstruction parameters and comparisons of the US-image based tumor-mimic volume estimations with reference tumor-mimic volumes (water displacement method).

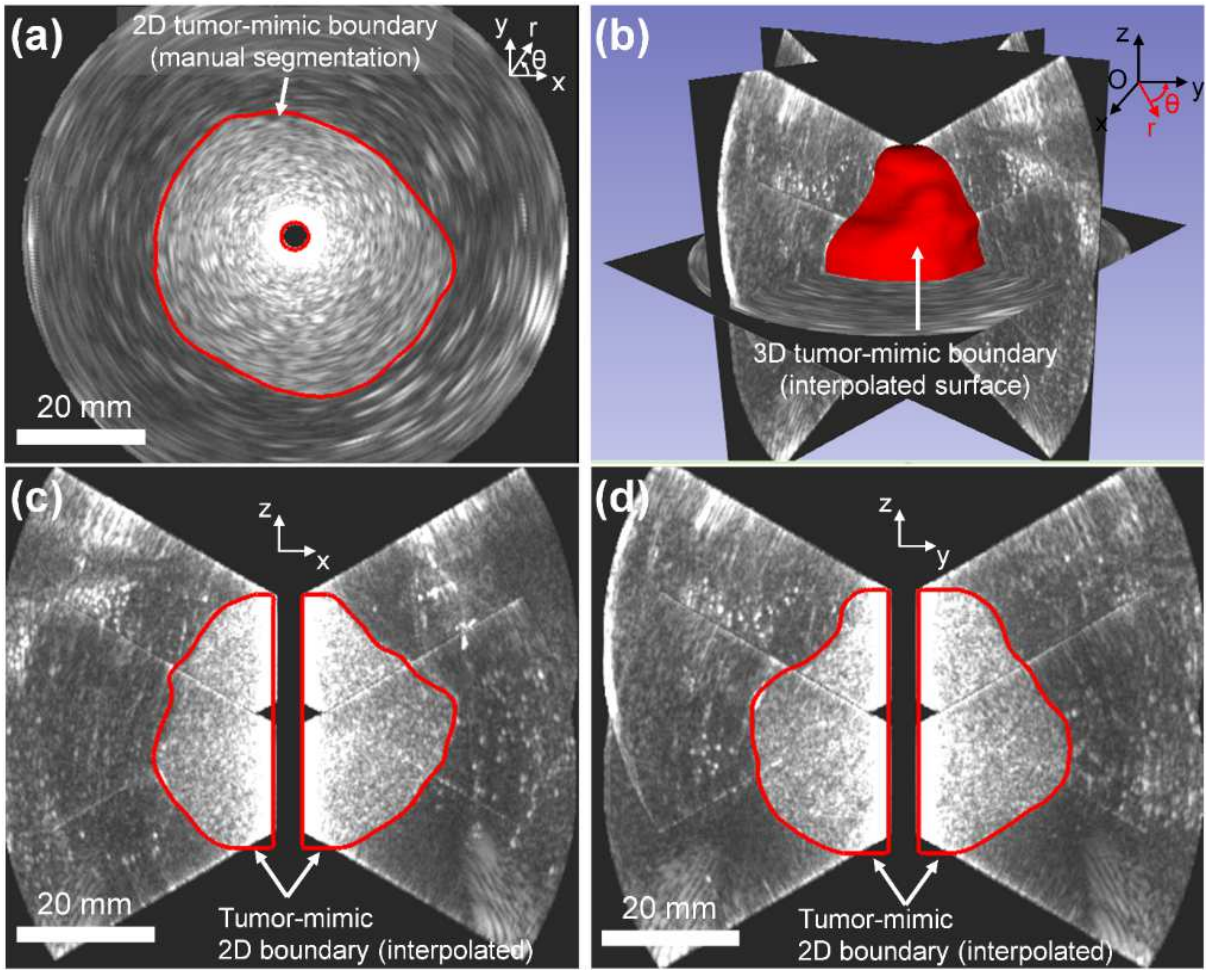

Fig. 7. Tumor-mimic model segmentation from the reconstructed 3D US image volume. Example where the USgHIFU prototype was inserted inside the tumor-mimic model (case #6). (**a**) Manual plan-by-plan tumor segmentation on the reconstructed azimuthal 2D US images (xOy plan). (**b**) 3D surface representing the 3D tumor boundaries, automatically created by interpolation over all 2D azimuthal segmentations. (**c**) View of the 2D elevational xOz plan. (**d**) View of the 2D elevational yOz plan.

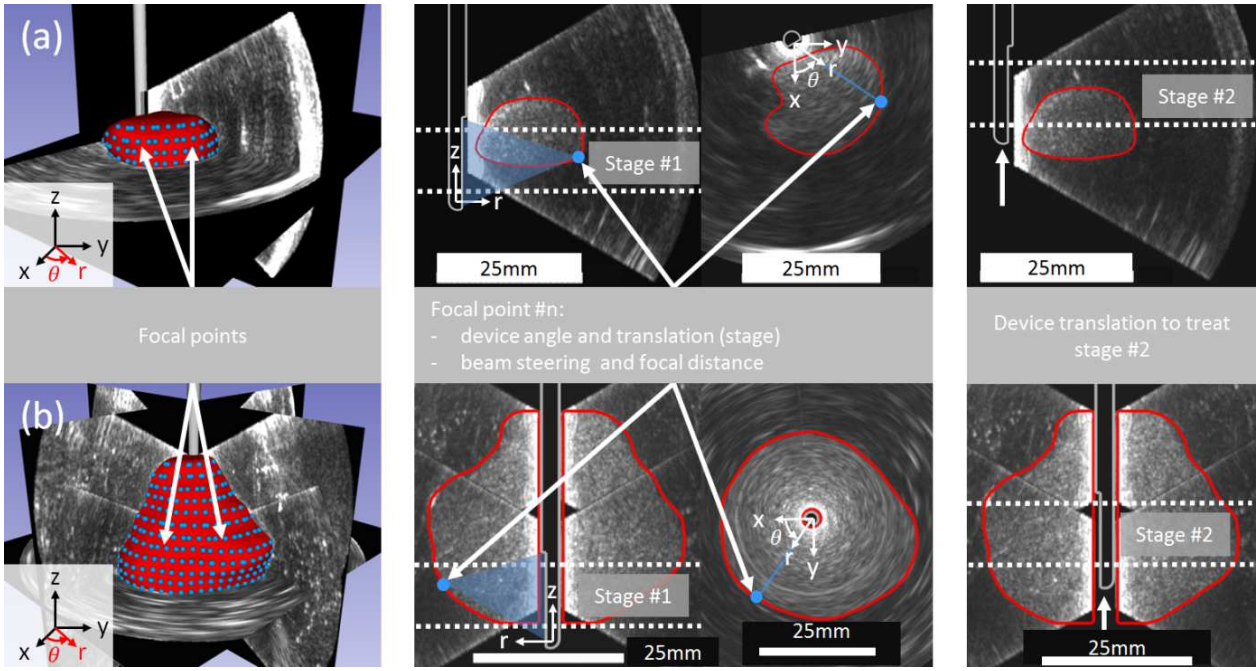

Fig. 8. Automatic HIFU treatment planning using the tumor-mimic model segmentations from the reconstructed 3D US image volume. (**a**) The USgHIFU prototype was inserted beside the tumor (Tumor-mimic #8). (**b**) The prototype was inserted inside the tumor (Tumor-mimic #6). In both cases, the left column shows the 3D view in the visualization software (3DSlicer) with the focal points (blue dots) mapping the tumor surface (red). Center column indicates the geometrical parameters defining a focal point: i) the ultrasound probe (grey) position is defined by two parameters, the device angle and translation; ii) the ultrasound focusing is also defined by to parameters, the beam steering and the focal distance. Left column illustrates that once a stage is treated the probe translate to treat the upper stage.

Tumor-mimic #	**1**	**2**	**3**	**4**	**5**	**6**	**7**	**8**
Interstitial prototype insertion	Beside the tumor	"	"	"	Inside the tumor	"	"	Beside the tumor
Tumor-mimic shape	Ovoid	"	"	"	"	"	Disc	"
Tumor-mimic volume, V_{US} (cm^3)	9.6	8.5	8.4	7.6	20.6	29.7	10.2	2.6
HIFU treatment volume (cm^3)	14.5	10.8	9.7	10.8	27.9	39.0	15.9	5.9
Under-treated volume (cm^3)	1.1	2.8	5.6	2.2	0.1	0.1	< 0.1	< 0.1
Under-treated volume (% of tumor volume)	11	33	67	30	< 0.5	< 0.5	< 0.5	2
Over-treated volume (cm^3)	6.0	5.1	7.0	5.4	7.3	9.4	5.7	3.4
Over-treated volume (% of tumor volume)	63	60	83	72	36	32	56	131
DSC	0.7	0.6	0.3	0.6	0.9	0.9	0.8	0.6
Treatment time (min)	44	35	34	32	78	124	40	14
Treatment rate (cm^3/min)	0.3	0.3	0.3	0.3	0.4	0.3	0.4	0.4
Number of treatment stage	3	3	3	3	4	4	2	2
Number of HIFU focal points	274	215	175	184	875	1118	497	93

Table 3: Interstitial conformal HIFU treatments of tumor-mimics in simulations. Summary of the metrics.

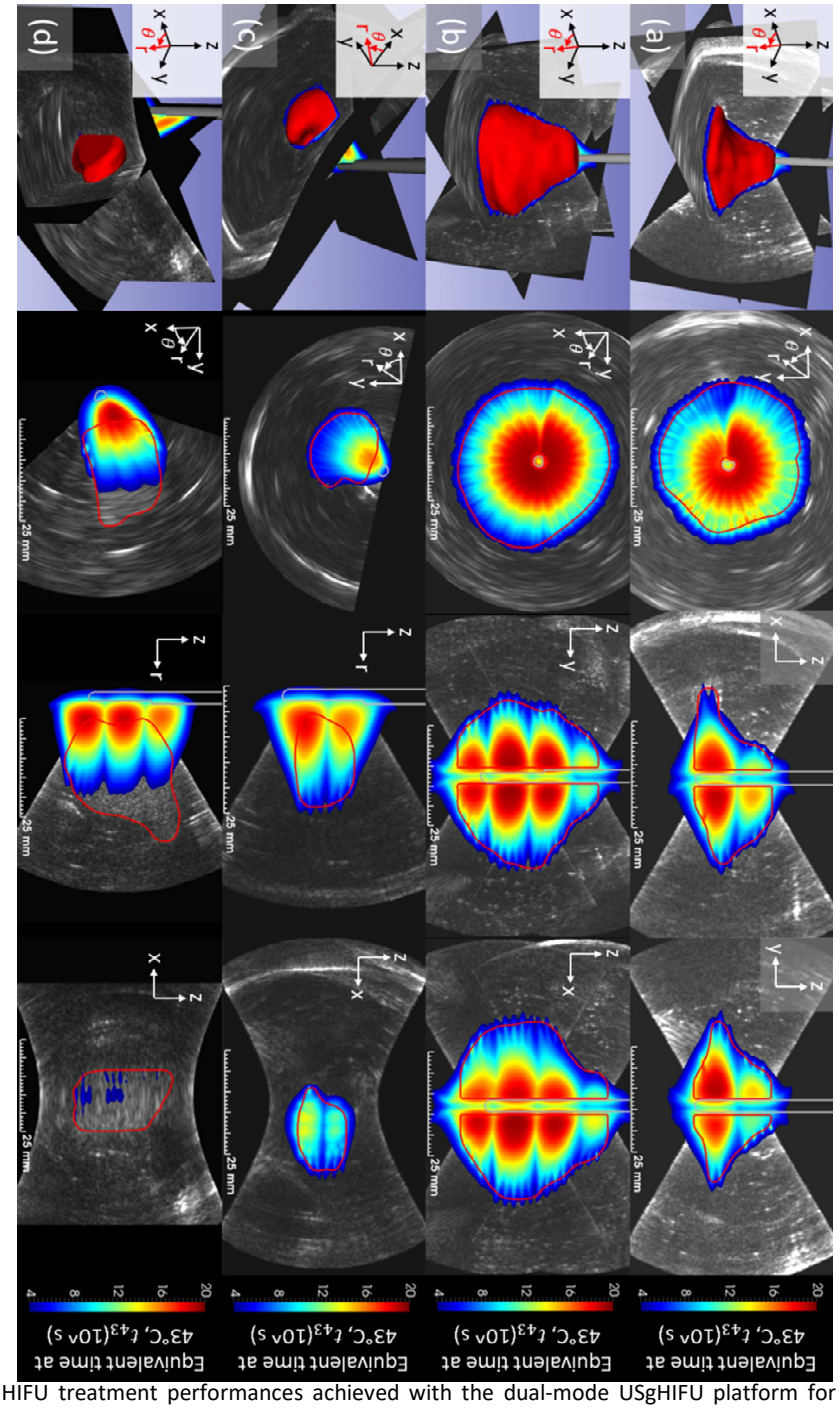

Fig. 9. Simulations of the HIFU treatment performances achieved with the dual-mode USgHIFU platform for conformal interstitial HIFU tumor ablation. The final thermal dose is overlaid on top of the US reconstructed 3D volume. Various HIFU treatment planning were obtained automatically using the US-image-based navigation guiding method presented in this study. (**a**-**b**) Cases of an interstitial device inserted inside the tumor. (**a**) Complete conformal treatment obtained in a disc-shaped tumor (diameter >> height) (tumor-mimic #7). (**b**) Complete conformal treatment obtained in an ovoid-shaped tumor requiring 4 stages of treatments (tumor-mimic #6). (**c**-**d**) Cases of an interstitial device inserted beside the tumor. (**c**) Complete conformal sectorial treatment obtained in a tumor ≤ 24 mm in diameter (tumor-mimic #8). (**d**) Incomplete conformal sectorial treatment obtained in a tumor > 24 mm in diameter (tumor-mimic #2).